



UNIVERSITY OF LEEDS

This is a repository copy of *Modeling the Stable Water Isotope Expression of El Niño in the Pliocene: Implications for the Interpretation of Proxy Data*.

White Rose Research Online URL for this paper:
<http://eprints.whiterose.ac.uk/120121/>

Version: Accepted Version

Article:

Tindall, JC, Haywood, AM orcid.org/0000-0001-7008-0534 and Thirumalai, K (2017) Modeling the Stable Water Isotope Expression of El Niño in the Pliocene: Implications for the Interpretation of Proxy Data. *Paleoceanography*, 32 (8). pp. 881-902. ISSN 0883-8305

<https://doi.org/10.1002/2016PA003059>

© 2017 American Geophysical Union. All Rights Reserved. This is an author produced version of a paper published in *Paleoceanography*. Uploaded with permission from the publisher.

Reuse

Unless indicated otherwise, fulltext items are protected by copyright with all rights reserved. The copyright exception in section 29 of the Copyright, Designs and Patents Act 1988 allows the making of a single copy solely for the purpose of non-commercial research or private study within the limits of fair dealing. The publisher or other rights-holder may allow further reproduction and re-use of this version - refer to the White Rose Research Online record for this item. Where records identify the publisher as the copyright holder, users can verify any specific terms of use on the publisher's website.

Takedown

If you consider content in White Rose Research Online to be in breach of UK law, please notify us by emailing eprints@whiterose.ac.uk including the URL of the record and the reason for the withdrawal request.



eprints@whiterose.ac.uk
<https://eprints.whiterose.ac.uk/>

Modeling the Stable Water Isotope Expression of El Niño in the Pliocene: Implications for the Interpretation of Proxy Data.

Julia C. Tindall¹, Alan M. Haywood¹ and Kaustubh Thirumalai²

Julia C Tindall, J.C.Tindall@leeds.ac.uk

¹School of Earth and Environment,
University of Leeds, Leeds, LS2 9JT, U.K.

²Institute for Geophysics, Jackson School
of Geosciences, University of Texas at
Austin, Austin, Texas, USA.

This article has been accepted for publication and undergone full peer review but has not been through the copyediting, typesetting, pagination and proofreading process, which may lead to differences between this version and the Version of Record. Please cite this article as doi: 10.1002/2016PA003059

Abstract. The El Niño Southern Oscillation (ENSO) drives interannual climate variability, hence its behavior over a range of climates needs to be understood. It is therefore important to verify that the paleoarchives, used for pre-instrumental ENSO studies, can accurately record ENSO signals.

Here we use the isotope enabled Hadley Centre General Circulation Model, HadCM3, to investigate ENSO signals in paleoarchives from a warm paleoclimate, the mid-Pliocene Warm Period (mPWP: 3.3-3.0Ma). Continuous (e.g. coral) and discrete (e.g. foraminifera) proxy data are simulated throughout the tropical Pacific, and ENSO events suggested by the pseudoproxy data are assessed using modeled ENSO indices.

HadCM3 suggests that the ability to reconstruct ENSO from coral data is predominantly dependant on location. However since modeled ENSO is slightly stronger in the mPWP than the preindustrial, ENSO is slightly easier to detect in mPWP aged coral.

HadCM3 also suggests that using statistics from a number of individual foraminifera (Individual Foraminifera Analysis; IFA), generally provides more accurate ENSO information for the mPWP than for the preindustrial, particularly in the Western and Central Pacific. However, a test case from the Eastern Pacific showed that for some locations the IFA method can work well

for the preindustrial but be unreliable for a different climate.

The work highlights that sites used for paleo ENSO analysis should be chosen with extreme care in order to avoid unreliable results. Although a site with good skill for preindustrial ENSO will usually have good skill for assessing mPWP ENSO, this is not always the case.

Keypoints:

- General Circulation Model used to simulate and interpret ENSO proxies of Pliocene age.
- Coral isotope data has similar skill at reconstructing ENSO for the Pliocene and the preindustrial.
- Regions where Individual Foraminifera Analysis can detect changes in Pliocene ENSO are considered.

1. Introduction

The El Niño Southern Oscillation (ENSO) is the strongest signal of interannual variability in the ocean-atmosphere system [Wang *et al.*, 1999]. Greater predictability of ENSO leads to greater predictability of weather extremes such as floods and droughts [Goddard and Dilley, 2005] and their associated socioeconomic impacts. However, there has been disagreement between models as to how ENSO will change in a warming climate [Latif and Keenlyside, 2009; Collins *et al.*, 2010; Bellenger *et al.*, 2014], and the future behavior of ENSO is uncertain.

One way to examine the dynamics of ENSO in a warmer than modern climate, is to examine warmer climates of the past. An interval that has received considerable attention is the mid-Pliocene Warm Period (mPWP). This occurred 3.264-3.025 Ma and represents a relatively familiar world with continental configuration similar to modern and CO₂ levels close to the current value of 400ppmv [Stap *et al.*, 2016; Seki *et al.*, 2010]. During the mPWP global annual mean surface temperatures were 2-3°C higher than the preindustrial era [Dowsett *et al.*, 2010; Haywood *et al.*, 2000] and polar ice volume was reduced by up to 1/3 [Dolan *et al.*, 2011].

The behavior of ENSO in the mPWP is subject to debate and uncertainty. However, unlike future ENSO uncertainties, there are datasets from the mPWP on which this debate can be assessed. Many studies have argued for protracted Pliocene El Niño conditions (referred to as a ‘permanent’ El Niño) [e.g. Molnar and Cane, 2002; Philander and Fe-

dorov, 2003; *Fedorov et al.*, 2006]. This has been based on lower productivity/reduced upwelling in the eastern equatorial Pacific [*Seki et al.*, 2012], regional climate patterns consistent with modern El Niño teleconnections [*Winnick et al.*, 2013], and perhaps most importantly a reduced east-west temperature gradient across the Pacific [e.g. *Wara et al.*, 2005]. This reduced east-west temperature gradient across the Pacific has been reconstructed using proxy data that suggests that the eastern equatorial Pacific (EEP) was warmer than today while the western equatorial Pacific (WEP) was not. However, *Zhang et al.* [2014a] used different proxies from the same WEP site which suggested that the WEP was also warmer than today and that a clear E-W temperature gradient existed during the Pliocene. Whether or not SST's in the WEP were warmer during the Pliocene, and hence whether a permanent El Niño is implied from this data is still not resolved [*Ravelo et al.*, 2014; *Zhang et al.*, 2014b; *Haywood et al.*, 2016].

Studies which support suggestions of a permanent Pliocene El Niño do not always suggest that this state was applicable to the whole of the Pliocene. For example *Steph et al.* [2010] suggested that the shallow thermocline and cold tongue in the EEP developed ~ 1 million years earlier in the Pliocene than was previously suggested. It is very likely that at least some of the Pliocene experienced ENSO variability. For example, *Watanabe et al.* [2011] found clear ENSO variability in two fossil corals from the Western Pacific, which were dated to approximately 3.5-3.8Ma. The fossil corals were analysed based on 12 samples per year for 35 years and so variability can be clearly measured. In addition *Scroxton et al.* [2011] found ENSO variability when considering measurements on individual plank-

tonic foraminifera.

Modeling studies generally agree that there was ENSO related variability in the Pliocene [Haywood *et al.*, 2007; Bonham *et al.*, 2009; von der Heydt *et al.*, 2011; Zhang *et al.*, 2012; Brierley, 2015]. However, simulations from complex atmosphere-ocean general circulation models (AOGCM's) represent only a short snapshot of the Pliocene, and do not apply to the whole Pliocene Epoch (5.33-2.58Ma). The time period most frequently modeled is generally representative of the mPWP (3.264-3.025Ma). In the same way that models do not agree on how ENSO behavior will change in the future, neither do they fully agree on how ENSO was different in the Pliocene. However, models do appear to share certain common features in their retrodiction of ENSO behavior. Brierley [2015] considered 9 models used in the Pliocene Model Intercomparison Project (PlioMIP), none of the models showed a 'permanent' El Niño, and there was a general consensus that there was less ENSO related variability with a shift to lower frequencies and reduced amplitude in the Pliocene. However Tindall *et al.* [2016] found that intra-model variability could exist within a single simulation, and suggested that there was likely to be centennial scale variability in mPWP ENSO strength in the same way that there is for the modern [Wittenberg, 2009; Li *et al.*, 2011]. Following a 2500 year spinup Tindall *et al.* [2016] found an increased amplitude of El Niño, even though there were shorter subsets of the simulation (200 years) in which the amplitude appeared to be reduced. It was found that the intramodel variability was particularly limited to temperature in the Eastern Pacific, and that the centennial scale variability was less important for precipitation or temperature in the central or western

Pacific.

Overall there are still substantial uncertainties in the behavior of Pliocene ENSO, and reducing these uncertainties could lead to a better understanding of ENSO in a warm climate. The uncertainties exist in both model and data, and it is difficult to compare the two due to the very different nature of what each can derive. GCM's provide climate indicators at a global scale for a relatively short timescale [e.g. 3.205Ma, *Haywood et al.*, 2013], while data is gathered from a very limited number of locations over a very long timescale [e.g. 'A 12 million-year temperature history...' *Zhang et al.*, 2012]. In addition the derived quantities are not always directly comparable. For example, the temperature and precipitation that is output from climate models is not directly measured in paleoarchives and is instead inferred from other quantities (e.g. Magnesium/Calcium ratios, alkenone unsaturation index, TEX₈₆ or the ratio of stable water isotopes). To better compare model and data it is necessary to either convert data measurements into quantities simulated by the model using a transfer function [e.g. *Erez and Luz*, 1983; *Dekens et al.*, 2002], or alternatively for the model to directly simulate the quantity measured in the geological archive. Recent years have seen a large increase in the number of models able to simulate measured quantities based on stable water isotope tracers, including global General Circulation Models [$\delta^{18}\text{O}$; e.g. *Lee et al.*, 2007; *Roche*, 2013; *Haese et al.*, 2013; *Dee et al.*, 2015] and a Regional Ocean Modeling System [*Stevenson et al.*, 2015]. This can be used to better compare model and $\delta^{18}\text{O}$ measured in paleoarchives [e.g. *Tindall et al.*, 2010; *Roberts et al.*, 2011; *Holmes et al.*, 2016]. For the mPWP, the Hadley Centre GCM, HadCM3, has been run with water isotope tracers included, to increase synergy

between model and data [*Tindall and Haywood, 2015*]. However, so far only the global large-scale features have been discussed.

Here we will use the water isotope enabled version of HadCM3 to investigate ENSO based on observed and simulated $\delta^{18}\text{O}$ in the Pacific ocean. The objectives are: 1. to compare model results with existing proxy data to investigate the potential accuracy of ENSO signals in the data, and 2. to directly simulate proxy measurements throughout the Pacific and suggest regions where proxy data of Pliocene age may provide a good representation of ENSO. For necessity we will limit model-data comparison to archives which contain $\delta^{18}\text{O}$ measurements and will also concentrate mainly on data with high temporal resolution, such as the coral data of *Watanabe et al. [2011]* and the individual planktonic foraminifera analysis of *Scroxton et al. [2011]*. This is because GCM's are run at very high temporal resolution and such a comparison allows a more comprehensive data-model comparison, which is not just based on one single datapoint in time.

In Section 2 we will describe the model and simulations used to simulate $\delta^{18}\text{O}$ for the Pliocene climate. Section 3 will discuss El Niño Southern Oscillation (ENSO) climate modes and show how these could appear in Pliocene climate $\delta^{18}\text{O}$ fields. Sections 4 and 5 will use the model results to reinterpret proxy data from corals and planktonic foraminifera respectively. In particular we will be assessing what information about ENSO can be derived from these archives, and locations where these archives would give the most reliable indication of El Niño behavior. A discussion of the results and the conclusions are pre-

sented in section 6.

2. Methods

2.1. Model description

The model used in this study is the Hadley Centre General Circulation Model [HadCM3; *Gordon et al.*, 2000; *Pope et al.*, 2000] with water isotope tracers included throughout the hydrological cycle [*Tindall et al.*, 2009]. HadCM3 has resolution of $3.75^\circ \times 2.5^\circ$ with 19 vertical levels in the atmosphere, and $1.25^\circ \times 1.25^\circ$ with 20 vertical levels in the ocean. HadCM3 uses the *Gregory and Rowntree* [1990] convection scheme, a large scale cloud scheme based on *Smith* [1990] with modifications described by *Gregory and Morris* [1996], and the *Edwards and Slingo* [1996] radiation scheme. In the ocean HadCM3 comprises a simple sea ice model, which is based on the zero-layer model of *Semtner* [1976] (and includes ice drifts, leads and snow cover). The version of the HadCM3 used here comprises the MOSES2 land surface exchange scheme which includes the TRIFFID dynamic vegetation model [*Cox et al.*, 1999] such that the vegetation is predicted by the model rather than prescribed.

HadCM3 has been used in a number of studies of the mPWP [e.g. *Hill*, 2015; *Pound et al.*, 2014; *Dolan et al.*, 2011] and in particular has been run as part of the Pliocene Model Intercomparison Project [PlioMIP; *Bragg et al.*, 2012; *Haywood et al.*, 2013]. HadCM3 is generally in good agreement with reconstructions although it underpredicts the Pliocene warming over the North Atlantic region [*Prescott et al.*, 2014] and the northern hemisphere high latitude terrestrial warming [*Salzmann et al.*, 2013]. The water isotope component of

HadCM3 has been shown to provide a good representation of the $\delta^{18}\text{O}$ of seawater ($\delta^{18}\text{O}_{sw}$) and the $\delta^{18}\text{O}$ of precipitation ($\delta^{18}\text{O}_p$) for the preindustrial climate [Tindall *et al.*, 2009], and has been used to investigate a variety of timeperiods including the large scale features of $\delta^{18}\text{O}_{sw}$ and $\delta^{18}\text{O}_p$ the mPWP [Tindall and Haywood, 2015].

For the modern HadCM3 simulates a reasonably good tropical Pacific climatology including the seasonal cycle of temperature and its interaction with wind stress [Guilyardi, 2006]. The seasonal cycle of tropical precipitation and $\delta^{18}\text{O}_p$ are also reasonable [Dai, 2006; Tindall *et al.*, 2009]. HadCM3 simulates a present day ENSO with amplitude and frequency broadly in agreement with observations, and its skill compares well with other CMIP3 and CMIP5 models [Bellenger *et al.*, 2014]. Although over much of the tropics precipitation anomalies compare well with observations [Dai and Wigley, 2000; AchutaRao and Sperber, 2002] the model fails to simulate the full area of dry conditions associated with El Niño that occur in the western Pacific warm pool. In HadCM3 precipitation amount is the main driver of $\delta^{18}\text{O}_p$ and $\delta^{18}\text{O}_{sw}$ in the tropical Pacific [Tindall *et al.*, 2009], therefore errors in regional precipitation ENSO signatures will propagate through to $\delta^{18}\text{O}_p$ and $\delta^{18}\text{O}_{sw}$. One example of how these errors are manifest was shown by Tindall *et al.* [2009] for a site (Madang 5°S, 145°E) in the western Pacific. In observations this site is drier in El Niño years because it is within the drier horseshoe shaped region which includes Northern Australia, Indonesia, Papua New Guinea and the Phillipines. In HadCM3 this site is wetter in El Niño years due to it being influenced by the enhanced convection region of the central Pacific, which, in HadCM3 extends too far west. This means that using HadCM3 to model coral $\delta^{18}\text{O}_c$ at this site, incorrectly suggests coral should be de-

pleted in $\delta^{18}\text{O}_c$ in El Niño years when in reality it is enriched. However further east where the model is able to accurately predict temperature and precipitation associated with El Niño, the model and data (including $\delta^{18}\text{O}_c$ coral) are in good agreement. Therefore care must be taken when using HadCM3 results to interpret paleodata from a fixed location (or paleoproxy site), and we suggest that the model results should be taken to be indicative of what an El Niño signal would look like in proxy data from a particular climate zone (i.e. wet, dry or warm region) as described in subsequent sections, rather than to suggest what El Niño would be like at small fixed locations. Alternatively if a site to model gridbox data-model comparison is required then it must first be ensured that the model is producing an accurate El Niño signal in at least temperature and precipitation for that model gridbox. Supplementary dataset 1 includes the typical climate for El Niño, La Niña and neutral conditions at each gridbox in the model in order that such a test can be performed.

2.2. Experimental Design

The HadCM3 experiments with $\delta^{18}\text{O}$ tracers analysed here were previously used by *Tindall and Haywood* [2015], and include a mPWP experiment and a preindustrial control. Both simulations were run for 2500 years and were initialised from a preindustrial experiment that had been run for several millenia with $\delta^{18}\text{O}$ tracers. The boundary conditions for the mPWP experiment are derived from the Pliocene Research, Interpretation and Synoptic Mapping project (PRISM), with ice sheets, orography and initial vegetation parameters from the PRISM3D version [*Dowsett et al.*, 2010]. This is intended to represent the interval between 3.264 and 3.025Ma. Orbital parameters are set to 3.205Ma [as

suggested by *Haywood et al.*, 2013] and CO₂ levels are set to 405ppmv.

The mPWP has been a focus of paleoclimate research for the past 25 years [*Dowsett et al.*, 2016] and as such the boundary conditions for these experiments are relatively well constrained compared to many other geological periods. However, there remain some uncertainties in the boundary conditions, and these are discussed in detail by *Dowsett et al.* [2010] and *Dowsett et al.* [2016]. The latest version of PRISM [PRISM4; *Dowsett et al.*, 2016] contains slightly different boundary conditions to what we use here and includes some changes to paleogeography and topography. In addition it also includes new databases of mPWP lakes and soils which are not the same as the preindustrial values used in our study. However sensitivity tests [*Pound et al.*, 2014] show that using mPWP lakes and soils only have a minor effect on the simulated climate in HadCM3.

Even though boundary conditions for the mPWP are uncertain there has been a concerted effort, via the Pliocene Model Intercomparison Project [PlioMIP *Haywood et al.*, 2010, 2011], to use a common set of boundary conditions in different models so that model retrodictions can be best compared. With common boundary conditions all models show a generally warmer world, with the increased temperatures amplified at the poles and an enhanced hydrological cycle. However there is intermodel disagreement as to the amplitude of the changes [*Haywood et al.*, 2013]. The largest intermodel uncertainty for temperature changes occurs at high latitudes, while the greatest intermodel uncertainty for precipitation changes occurs in the tropics. There are also areas of model-data disagreement, such as a modeled cold bias in the Northern Hemisphere [*Salzmann et al.*, 2013], which could

be partially due to the data used in the reconstructions spanning several orbital cycles, while model results are often based on a fixed orbit [Prescott *et al.*, 2014].

On glacial timescales, globally averaged $\delta^{18}\text{O}_{sw}$ is dependent on the amount of low $\delta^{18}\text{O}$ water that is stored in the ice sheets, which is largely determined by ice volume. Since the mPWP ice volume was reduced relative to the preindustrial, yet the mPWP simulation initialised $\delta^{18}\text{O}_{sw}$ from a preindustrial simulation, the simulated mPWP $\delta^{18}\text{O}_{sw}$ has been corrected at a post-processing stage. Following Tindall and Haywood [2015], a uniform reduction of 0.3‰ has been applied to simulated mPWP $\delta^{18}\text{O}_{sw}$, to account for a reduction in ice sheet volume (relative to the preindustrial) of 1/3 and a corresponding sea level rise of 28m. This correction is included in all figures throughout this paper, however since there is some uncertainty over the exact value of Pliocene sea level [Miller *et al.*, 2012] this value could be changed, if required, as estimates are refined.

3. The El Niño Southern Oscillation in the mPWP

El Niño and La Niña months were detected in these simulations based on the Oceanic Niño Index (ONI), which is used by NOAA's Climate Prediction Center. The ONI is the three month running mean SST anomaly in the NINO3.4 region (5°N-5°S, 170°W-120°W); when the ONI exceeds a threshold of +0.5°C for at least 5 consecutive months it is categorised as El Niño, when the ONI is below -0.5°C for at least 5 consecutive months it is categorised as La Niña. Months that are neither El Niño or La Niña are categorised as 'neutral'. Figure 1 shows the temperature, precipitation, $\delta^{18}\text{O}_p$ and $\delta^{18}\text{O}_{sw}$ anomalies for an El Niño composite minus a neutral composite, for the preindustrial (left), the mPWP

(center) and the difference between them (right). Here El Niño/neutral composites have been produced using a weighted average of all El Niño/neutral months such that a composite includes the same amount of information from each month of the year. It is seen that for all fields considered the HadCM3 El Niño anomaly is stronger in the mPWP than in the preindustrial. Relative to the preindustrial the magnitude of the mPWP El Niño anomaly is approximately 28% larger for temperature, 32% larger for precipitation, 29% larger for $\delta^{18}\text{O}_p$ and 37% larger for $\delta^{18}\text{O}_{sw}$, although there is spatial variability in these numbers (particularly for temperature). We note that figure 1 is typical for years 1500-2500 of the simulations however in a small number of earlier centuries of the simulation ENSO was found to be weaker in the mPWP in the NINO3.4 region [despite continuing to be stronger elsewhere; *Tindall et al.*, 2016]. If we assume that the increase in mPWP ENSO strength shown in figure 1 is reasonable, this suggests that, unless the amplitude of non-ENSO climate signals has similarly increased, the signal to noise ratio of ENSO events in the mPWP was larger than the preindustrial and may be more easily detectable in mPWP aged proxy data.

Supplementary figure 1 is analogous to figure 1 but shows seasonal (DJF-JJA) anomalies of temperature, precipitation $\delta^{18}\text{O}_p$ and $\delta^{18}\text{O}_{sw}$ for the preindustrial, the mPWP and the mPWP-preindustrial difference. The mPWP-preindustrial seasonal anomalies have been plotted on the same scale as figure 1 in order to aid comparison. Because the mPWP simulation used an orbit that is similar to modern, the seasonal cycle is similar between the two time periods, however in some regions and for some fields (e.g. $\delta^{18}\text{O}_{sw}$ in parts of the western equatorial Pacific) the change in the annual cycle between the two climates

could be larger than the change in ENSO. If the method of proxy interpretation is not able to remove the effects of the annual cycle the signal to noise ratio of ENSO events in these regions could be reduced in the mPWP relative to the preindustrial and ENSO may be more difficult to detect in mPWP aged proxy data. This will be discussed further in section 5.2, however there are already indications that whether ENSO is easier or more difficult to detect in mPWP aged data could be strongly location dependent.

In the next sections we will discuss how the El Niño temperature and $\delta^{18}\text{O}_{sw}$ signals seen in HadCM3 would combine within a proxy archive and what information about ENSO we would be able to gather from that archive. In particular we discuss whether the ability to detect ENSO in $\delta^{18}\text{O}$ measured in a mPWP archive is likely to be different from the preindustrial.

4. ENSO signals in Coral Data

To assess El Niño, it is beneficial to have climate proxy data of high temporal resolution. The coral data of *Watanabe et al.* [2011] (extracted from two 35 year corals in the Philippines) has monthly resolution - which is the highest available for the Pliocene. A spectral analysis of the $\delta^{18}\text{O}$ of these corals showed spectral peaks that correspond to present day ENSO variability. In addition $\delta^{18}\text{O}$ from a nearby, live, coral correlated well with modern records of ENSO and negative $\delta^{18}\text{O}$ events in the fossil coral resemble negative $\delta^{18}\text{O}$ events in the live coral. The evidence from these corals suggest Pliocene ENSO variability similar to modern.

In theory, this coral data is ideal for validating the HadCM3 mPWP isotope simulations and also for combining model and data to better understand mPWP El Niño. However these corals are from a region of the Western Pacific where HadCM3 fails to reproduce the dry conditions associated with El Niño, either for the mPWP or the preindustrial (see star on figure 1). At this gridbox the model is therefore unable to produce the spectral peaks at ENSO frequencies that are seen in the data (supplementary figure 2). As discussed in section 2.1, a site to model-gridbox data-model comparison should not be used to assess ENSO at a location such as this where the modeled ENSO patterns are inaccurate. To understand what information about ENSO could be determined from coral in a region with a ‘dry’ El Niño signal, an alternative region of the Pacific where El Niño precipitation patterns are better represented by the model will later be discussed. We note that a region in the Western Pacific of HadCM3 which has a dry El Niño signal is more appropriate for assessing the ENSO signature of corals from a dry El Niño location than the nearest gridbox if the nearest gridbox does not have a dry El Niño signal.

However, the *Watanabe et al.* [2011] coral data is a unique resource for our study, and should therefore be utilised as much as possible. Here it is used to validate the annual average and non-ENSO (e.g. seasonal) related variability of $\delta^{18}\text{O}_c$ simulated by the model. Figure 2 compares the coral data of *Watanabe et al.* [2011], to HadCM3 pseudocoral $\delta^{18}\text{O}_c$ produced from the nearest gridbox (14.375°N, 124°E). Shown is the mean annual cycle (dashed line) and the annual cycle ± 2 standard deviations (grey shaded area) corresponding to the approximate 95% confidence interval. The pseudocoral

$\delta^{18}\text{O}_c$ (figure 2c) was produced by combining modeled temperature with modeled $\delta^{18}\text{O}_{sw}$ according to the equation of *Juillet-Leclerc and Schmidt* [2001] which is:

$$T = 2.25 - 5(\delta^{18}\text{O}_c - \delta^{18}\text{O}_{sw}). \quad (1)$$

The thin black lines on figure 2c show the values within 2 standard deviations of the mean calculated using the last 35 years of the simulation (corresponding to the length of the *Watanabe et al.* [2011] coral), while the green lines show the values within 2 standard deviations calculated using the last 300 years of the simulation. This confirms that variation in the modeled annual cycle compare well with the data and is robust over a longer time period.

Even though the spectral peaks at ENSO frequencies that occurs in the coral data is absent from our pseudocoral $\delta^{18}\text{O}_c$ (supplementary figure 2), there appears to be excellent model-data agreement on seasonal timescales at this location. The general agreement between the *Watanabe et al.* [2011] coral and HadCM3 (figure 2) suggests that the model is able to provide a good representation of coral data of mPWP age.

In order to use HadCM3 for interpreting coral ENSO signals we now derive HadCM3 pseudo-corals from other locations, where the model better represents El Niño. These locations are shown on figure 1 and are: two locations where there is a large temperature signal associated with ENSO (a) in the central Pacific (0°N , 190°E ; circle) and b) in the Eastern Pacific (7°S , 81°W ; square); c) a gridbox in the Western Pacific (3°S , 141°E ; triangle) which has increased precipitation (and hence a negative $\delta^{18}\text{O}_{sw}$ excursion) in El

Niño years and d) a gridbox (16°S, 175°E; diamond) which has reduced precipitation in El Niño years. At each of these locations pseudocoral $\delta^{18}\text{O}_c$ is produced using equation 1.

Figure 3 shows the power spectral density of $\delta^{18}\text{O}_c$ from a 300 year pseudocoral at each location. This has been normalised by dividing by the variance of the coral $\delta^{18}\text{O}_c$ and the frequency resolution (1/300 cycles per year) such that the sum of power over the all calculated frequencies (0-6 cycles per year) is 1.0. The power spectrum has also been smoothed using a 10 point running mean for clarity and the shaded bars show frequencies representing the 2-7 year period of expected ENSO variability. Since the pseudo-corals lie in ENSO regions they all exhibit spectral peaks at ENSO frequencies. However, the spectral peaks are not the same in every pseudo-coral, which implies that the skill of each pseudocoral in detecting ENSO signals will be different. Of these pseudocorals the strongest spectral peaks in $\delta^{18}\text{O}_c$ lie in the central pacific (figure 3a), and at the site with reduced precipitation in El Niño years (figure 3d) while the weakest spectral peaks are in the Eastern Pacific (figure 3b) and the site with increased precipitation in El Niño years (figure 3c). Supplementary figures 3 and 4 are analogous to figure 3, but show the power spectral density of $\delta^{18}\text{O}_{sw}$ and temperature respectively. As expected, spectral peaks in figures 3a and b are due to the temperature component of the coral, while spectral peaks in figures 3c and d are mainly due to the $\delta^{18}\text{O}_{sw}$ component of the coral. However there are also notable spectral peaks in temperature at the 'dry El Niño' site (supplementary figure 4d).

We now consider whether true El Niño and La Niña events can be detected from any of these pseudo corals, and the likely accuracy in detection. For each of the four sites we show the final 50 years of the pseudocoral $\delta^{18}\text{O}_c$ after removal of the average annual cycle (black line figure 4). El Niño and La Niña events were then inferred if the pseudocoral $\delta^{18}\text{O}_c$ was more extreme than a threshold, t_{ENSO} , for at least 6 consecutive months. The threshold, t_{ENSO} was taken to be one half of the standard deviation of the pseudocoral $\delta^{18}\text{O}_c$; it is the same threshold used by *McGregor et al.* [2010], who noted that it is roughly consistent with the SSTA threshold used for the definition of ENSO events by NOAA (0.5°C above or below the mean state calculated from the period 1971-2000, where the standard deviation of observed NINO3.4 region SSTA for the period 1971-2000 is 0.93°C).

Times of the simulation when the pseudo-coral infers El Niño and La Niña are shown as red bars (El Niño) and blue bars (La Niña) that are plotted below the x-axis in figure 4. It can be seen that El Niño and La Niña are more often suggested by the simulation at location d) than elsewhere, while the pseudocoral at the central Pacific location (a) suggests less and generally shorter duration El Niño. Despite a notable overlap the same ENSO state is not inferred from the different pseudocorals.

A main advantage of using a climate model to simulate paleodata is that the model can simulate other climate features that occur simultaneously with the modeled paleodata. In this case ‘true’ El Niño and La Niña determined from the ONI can be obtained. Times when the model was in a ‘true’ state of El Niño and La Niña, are shown by the red and blue bars above the x-axis on figure 4. This means that bands which occur above and

below the x-axis represent times when El Niño or La Niña has been correctly detected from the pseudocoral $\delta^{18}\text{O}_c$, bands that occur only above the axis represent times that El Niño or La Niña occurred in the model that could not be detected in the pseudocoral and bands that occur only below the x-axis represent times that the pseudo coral falsely suggests an El Niño or La Niña event. It can be seen that figure 4(a) which represents the central Pacific location is the point where El Niño can be best detected, here all events within the 50 years shown are correctly detected and few false events are inferred. At the other locations most of the El Niño/La Niña events are also correctly detected within the pseudocoral data, however there are a large number of events predicted that did not occur, particularly for the dry El Niño location (d).

The large number of false events seen on figure 4 questions whether the threshold chosen to infer ENSO was too low. It is noted that the exact threshold is unknown, and will likely change depending on the location of the pseudo-coral and the time period. We note that an alternative threshold may have been more appropriate for some locations, and it is possible to optimise the threshold by calculating which threshold gives the maximum number of correctly attributed ENSO states [*Hereid et al.*, 2013]. However here we have chosen not to optimise the threshold value as such optimisation is not possible with paleodata of mPWP age. Also, the condition that the extreme values must persist for 6 consecutive months reduces the importance of the exact threshold chosen.

To extend the results from figure 4 we consider the number of El Niño and La Niña events that can be detected in the final 300 years of the mPWP simulation. This is shown

in Table 1, and supports the results in figure 4. Most of the El Niño and La Niña events within the 300 years can be detected using this method (albeit with a number of false positives).

For comparison table 1 also shows the number of ENSO events that could be detected in the corresponding preindustrial simulation. It can be seen that overall a greater proportion of El Niño and La Niña can be detected in the mPWP pseudocorals (average 88%) than in corresponding preindustrial pseudocorals (average 81%) and the percentage of events predicted in error is smaller in the mPWP (average 32%) than in the preindustrial (average 42%). The reason that El Niño events are easier to detect, from a single site, in the mPWP than in the preindustrial is due to the fact that El Niño events are stronger, relative to the background variability in the mPWP. There is also notable coherence between the mPWP and the preindustrial results: those sites which have good skill for the preindustrial also have good skill for the mPWP. If the results of this modeling study accurately represent ENSO behavior, they suggest that ENSO can usually be detected from a single site in the mPWP provided the site is suitable for detecting modern ENSO.

Table 1 and figure 4 both show the skill to be best at the central Pacific site (a), followed by the Eastern Pacific site (b). The sites with an ENSO precipitation signal (c and d) appear to show similar skill in table 1, which just compares the number of events. However from figure 4 the skill appears better at site c (which has increased precipitation in El Niño years) because the false positives at this location are of shorter duration. Considering these four sites only, the skill of ENSO detection appears only loosely related

to the strength of the spectral peaks seen in figure 3. Although the spectral peaks were strongest in the central Pacific site (which had best skill) the spectral peaks were weakest in the Eastern Pacific site where the skill was also relatively good.

4.1. Application across the Tropical Pacific

The ability to detect ENSO in pseudocorals has so far been discussed in relation to four locations where there is a strong ENSO signal and good skill is expected. However the model is not limited to four locations. We are able to calculate $\delta^{18}\text{O}$ from many pseudocoral to fully investigate where the model suggests there should be a strong and accurate ENSO signature in timeseries data of mPWP age. We therefore produce a 500 year pseudo-coral using equation 1 for each gridbox across the Pacific. To compare locations each pseudocoral will be allocated a skill score based on its ability to detect ENSO. The skill score for each pseudocoral is calculated as follows:

$$skill = \left(\frac{1}{3} \left[\frac{EN_c}{EN_t} + \frac{LN_c}{LN_t} + \frac{NT_c}{NT_t} \right] - \frac{1}{3} \right) \times \frac{2}{3} \quad (2)$$

where EN, LN and NT denote the number of El Niño, La Niña and neutral months respectively. c denotes the number of months of each type that were correctly attributed and subscript t denotes the total months of that type. Note that the skill score has been normalised by subtracting $1/3$ from the average of correctly detected events and multiplying by $2/3$. Normalising means that if the model performs no better than random chance, there is an expected skill of 0 and perfect predictability will have a skill of 1. Also note that when determining whether a month was correctly attributed a two month margin of

error was allowed, such that a month would be classed as correctly attributed if it was within 2 months of the predicted state.

The skill of the pseudo corals across the Pacific is shown in figure 5 for the preindustrial and the mPWP. As expected from our four test pseudocorals, regions of high skill in the preindustrial generally correspond to regions of high skill in the mPWP, and the difference in skill between regions is much larger than the difference in skill between the two time periods even though overall skill is slightly better in the mPWP. However because the model is subject to uncertainty both for the mPWP and the preindustrial, and because the representation of ENSO is not perfect (particularly in Western Pacific precipitation) figure 5 should be taken as indicative of whether ENSO can be detected in a particular climate region (i.e. warm/dry/wet) instead of whether ENSO can be detected at a particular gridbox. Despite the uncertainties, this work strongly suggests that if ENSO can be determined from time series data at a modern site, then the site is also appropriate for detecting ENSO in time series data of mPWP age.

5. Comparison to planktonic foraminifera data

5.1. Bulk Foraminifera measurements

Although not able to provide a timeseries in the same way as coral data, previous work has used planktonic foraminifera data to assess El Niño changes between the Pliocene and the modern. Planktonic foraminifera data has been used in two main ways: 1.) a Bulk Foraminifera analysis where a number of foraminifera are crushed and mixed before analysis to find typical climate conditions. Data from bulk foraminifera analysis will be

discussed in this section. 2.) an individual foraminifer analysis, where a number of single foraminifera are used to find the variability in climate. This will be discussed in section 5.2.

Wara et al. [2005] considered bulk foraminifera data from two sites, one from the Eastern Pacific and one from the Western Pacific. These suggested that the average temperature gradient across the Pacific was smaller in the Pliocene than the modern (2°C in the Pliocene, 6°C modern). They noted that the Pliocene average gradient was similar to modern “El Niño” conditions, and hypothesised that the Pliocene was in a permanent El Niño-like state. However, their study also suggested that the thermocline depth in the Eastern Pacific from 4Ma-0Ma was similar to today, and not indicative of a permanent El Niño over this period. A permanent El Niño condition in the mid-Pliocene Warm Period does not agree with modeling studies [*Bonham et al.*, 2009; *Brierley*, 2015] or some other analyses [*Zhang et al.*, 2014a]. Since this paper includes modeling of $\delta^{18}\text{O}$ in planktonic foraminiferal calcite (hereafter referred to as $\delta^{18}\text{O}_F$), we revisit the comparison between the HadCM3 model and the *Wara et al.* [2005] study, in order to see if the two can be better reconciled.

The sites used in the *Wara et al.* [2005] study were ODP 806 (0°N,159°E) in the Western Pacific and ODP 847 (0°N,95°W) in the Eastern Pacific. Site ODP806 is the only published data of Pliocene age from the WEP warm pool [*Ravelo et al.*, 2014] and there is a great deal of controversy as to whether or not this site was warmer than modern [*Ravelo et al.*, 2014; *Zhang et al.*, 2014b]. Although most of this debate has been focussed on the early Pliocene (3.5-5Ma ago), the reasoning can extend to the mPWP timeslice considered

here. There is less controversy in the EEP. Studies generally agree that in the Pliocene this region was warmer than today. Due to a lack of data of Pliocene age, the sites used in the *Wara et al.* [2005] study are important locations for considering discrepancies in ‘permanent El Niño’ indicators.

Preindustrial HadCM3 does not reproduce the modern 6°C temperature difference calculated by *Wara et al.* [2005] between ODP806 and ODP847. Instead HadCM3 shows a temperature difference of 0.5°C at the surface and 4°C at 20m (20m being the depth represented by the data). The discrepancy is partly due to the location of the sites. The Eastern Pacific site is located on the edge of the cold tongue in an area of large horizontal temperature gradients, while the location of the Western Pacific warm pool is slightly offset in HadCM3, meaning that in HadCM3 the Western Pacific site is not representative of the Western Pacific warm pool. Because of these issues we do not perform a site to model gridbox model data comparison here. Instead we will consider the range of values that lie within 2.5° and 5° of the gridbox containing each site, which will ensure that both the cold tongue and the warm pool in HadCM3 are included.

Figure 6 shows the range of modeled values of $\delta^{18}O_F$ and temperature within 2.5° and 5° of the western Pacific warm pool region (blue) and the Eastern Pacific region (hatched) for the preindustrial simulation and the mPWP simulation. $\delta^{18}O_F$ was obtained from modeled temperature and modeled $\delta^{18}O_{sw}$ using the equation of *Erez and Luz* [1983]:

$$T = 17.0 - 4.52(\delta^{18}O_F - \delta^{18}O_{sw}) + 0.03(\delta^{18}O_F - \delta^{18}O_{sw})^2. \quad (3)$$

Preindustrial $\delta^{18}\text{O}_F$ is in reasonable agreement with the core top values, which represent recent times, [-2.22‰ at site 806 and -1.42‰ at a location near site ODP847 *Dekens et al.*, 2002]. However the modeled 20m depth $\delta^{18}\text{O}_F$ at 3.2Ma is less than *Wara et al.* [2005] reported for site ODP806 ($\sim -1.44\text{‰}$) or site 847 ($\sim -1.23\text{‰}$). Despite this notable offset the measured gradients across the Pacific of 0.21‰ is within the large range of gradients across the Pacific calculated using values that occur within 2.5° of the modeled sites (-1.37‰ - 0.01‰). Also the gradients across the Pacific calculated using values that occur within 2.5° of the modeled sites for the mPWP (1.2°C - 7°C) and the preindustrial (0.9°C - 7.3°C) encompasses the observations (2°C in the Pliocene, 6°C modern). However, in the model the temperature and $\delta^{18}\text{O}_F$ gradients at these locations, are similar for the two time periods, while in the data they are not. In agreement with *Wara et al.* [2005] the thermocline in the Eastern Pacific is similar for both the preindustrial and the mPWP. The main differences between the two time periods is a $\sim 0.5\text{‰}$ decrease in $\delta^{18}\text{O}_F$ and a $\sim 2.0^\circ\text{C}$ warming in the mPWP which applies consistently to the top 100m of the ocean and at both sites. The model is unable to assess why some analyses show the Western Pacific was warmer in the Pliocene, while others do not. We are not able to corroborate suggestions by *Zhang et al.* [2014a], that some records could have been compromised by changes in seawater chemistry, diagenesis and calibration limitations. However we do note the $\delta^{18}\text{O}_F$ Pliocene data is up to 1.2‰ higher than in the model, while the model agrees well with data for recent times, opening the possibility that diagenesis may be

affecting at least the $\delta^{18}\text{O}_F$ measurements.

The large temperature gradients across both sites and the strong Eastern Pacific thermocline means that a small shift in either the Warm Pool or the cold tongue could lead to a reduction in the gradient across the Pacific without a permanent El Niño. Although we do not see either feature shift in our simulations it is possible that a different (and equally valid) orbital configuration which occurred in the Pliocene may lead to such a shift. Attributing a reduced E-W gradient (based on a single Western Pacific site) to ‘permanent’ El Niño, is not robust, even if the existence of such an E-W gradient were universally accepted.

5.2. Individual Foraminifera Analysis (IFA)

The major limitation of using bulk foraminifera measurements to investigate El Niño for past climates is that interannual variability can not be measured. For example although bulk foraminifera measurements can suggest whether or not the average East-West temperature gradient in the Pliocene was different, they cannot indicate why these average differences occur. For example a smaller east-west average temperature gradient could be due to: a) a permanent “El Niño like” condition b) ENSO variability around a smaller than modern East-West temperature gradient, or c) more frequent and stronger El Niño episodes imposed on a background state similar to modern. To overcome these issues an alternative way of analysing foraminifera was proposed by *Koutavas et al.* [2006]. This analyses $\delta^{18}\text{O}_F$ measurements on a number of individual foraminifera, with a single foraminifera representing the climatic conditions for a 2-4 week period. While the exact

age of the sample and the calendar month it represents is unknown and indeterminable, a large number of individual foraminifera measurements can show the range of monthly variability in a paleoclimate. The warmest measurements will likely represent the warmest calendar month and the coldest measurements will likely represent the coldest calendar month. Any foraminifera representing temperatures that lie outside of the expected seasonal range are classed as ‘extra seasonal’ and can be theoretically attributed to ENSO related variability. This method has the disadvantage that it can only detect El Niño in months that are more extreme than the seasonal cycle, and is further complicated by the fact that sedimentation rates at a location may restrict the number of samples available to represent the population for a short time interval [Thirumalai *et al.*, 2013]. For example, a very large El Niño in September would not show extraseasonal temperature in the Eastern Pacific region, since it would still be cooler than the average April temperature. The advantage to this method is that some El Niño and La Niña events should be detected, provided enough individual foraminifera are used, and the presence of these events should be sufficient to state whether there was ENSO variability. Here we use the HadCM3 simulations to investigate whether ENSO variability in the mPWP can be detected in this way and compare results to the *Scroxton et al.* [2011] study which analysed individual foraminifera of Pliocene age to determine ENSO variability.

HadCM3 is used to simulate values of individual foraminifera $\delta^{18}\text{O}_F$ using equation 3 at the gridbox containing the ODP site 846 (3°S,90°W) that was used by *Scroxton et al.* [2011]. This is shown for the mPWP and the preindustrial in figure 7. Here each foraminifera $\delta^{18}\text{O}_F$ is calculated using the temperature and $\delta^{18}\text{O}_{sw}$ that occurred in a sin-

gle month of the last 50 years of the simulation. Black crosses represent times when the model was in a neutral state, red crosses represent times when the model was in an El Niño state and blue crosses represent times when the model was in a La Niña state. Different depths have been shown to suggest what the results would be for different foraminifera species, and foraminifera representing El Niño and La Niña have been slightly offset for clarity. For the preindustrial (figure 7a), it can be seen that the extreme low $\delta^{18}\text{O}_F$ values represent times when the model is in an El Niño state, while the extreme high $\delta^{18}\text{O}_F$ values represent times when the model is in a La Niña state. This analysis suggests that, for the preindustrial, extraseasonal events detected in Planktonic foraminifera species that live down to 130m, will represent El Niño and La Niña conditions.

For the mPWP (figure 7b) the results are slightly different. In this case the times with extraseasonal high values of $\delta^{18}\text{O}_F$ still generally represent La Niña conditions, however the times of extraseasonal low values of $\delta^{18}\text{O}_F$ is less clear than the preindustrial case. Indeed this figure suggests that in the top 30m of the ocean the times of greatest extraseasonal low values of $\delta^{18}\text{O}_F$ are associated with La Niña which is contrary to expectations. Although both extraseasonal high and low values of $\delta^{18}\text{O}_F$ are reproduced by the mPWP simulation (seen on figure 7b as the small proportion of El Niño and La Niña months which are not within the range of the ‘neutral’ annual cycle), without prior knowledge it would be impossible to accurately determine El Niño events from the simulated foraminifera data. In order to check that the last 50 years of the mPWP simulation were typical, we repeated this analysis for the preceding 50 years of the mPWP simulation and found similar results (supplementary figure 5). However in the preceding 50 years extraseasonal

low values of modeled $\delta^{18}\text{O}_F$, at the time of La Niña, were also obtained down to the 130m depth.

To understand why the model suggests it possible to detect extraseasonal El Niño events in the preindustrial, but not in the mPWP, at this site we will first consider the component parts of the modeled foraminifera $\delta^{18}\text{O}_F$, namely $\delta^{18}\text{O}_{sw}$ and temperature. We will consider the surface and also the next layer (10-20m) where the extraseasonal low values occurring at the time of a La Niña are highest.

Figure 8a shows the timeseries of monthly averaged temperature, $\delta^{18}\text{O}_{sw}$ and $\delta^{18}\text{O}_F$ which corresponds to figure 7 for the preindustrial simulation. Times where the model is in an El Niño state are shown in red, times when the model is in a La Niña state are shown in blue and neutral conditions are shown in black. Horizontal lines have been overplotted at arbitrary limits of 28°C for temperature, 0.7‰ for $\delta^{18}\text{O}_{sw}$ and -2.6‰ for $\delta^{18}\text{O}_F$ to highlight where the extreme values occur. In agreement with figure 7 we see that the times of lowest $\delta^{18}\text{O}_F$ values occur during El Niño conditions, the highest $\delta^{18}\text{O}_F$ occur during La Niña condition and extraseasonal values are correctly attributed. The low values of $\delta^{18}\text{O}_F$ that are detected as El Niño are all due to warm temperatures and $\delta^{18}\text{O}_{sw}$ varies little (standard deviation=0.05‰). Figure 8b shows the analogous timeseries for the mPWP simulation. Although generally the highest temperature values occur at the time of an El Niño and the lowest temperature values occur at the time of a La Niña, these results do not always follow through into $\delta^{18}\text{O}_F$. Indeed the most extreme low values of $\delta^{18}\text{O}_F$ occur around months 16-17 (year 2) at a time of La Niña (see also extreme value at 10m on

figure 7b). In addition some true El Niño episodes which cause extreme values in temperature do not translate to extreme values in $\delta^{18}\text{O}_F$ (see year 17). These errors are partly due to temperature (which will be discussed later) and partly due to changes in $\delta^{18}\text{O}_{sw}$.

Comparing figures 8a and 8b we see that $\delta^{18}\text{O}_{sw}$ at this site was much more variable in the mPWP (standard deviation 0.07‰). Variability in $\delta^{18}\text{O}_{sw}$ is clearly not tied to the phase of ENSO, however an extreme low value of $\delta^{18}\text{O}_{sw}$ (such as occurs at months 16-17) can amplify a small peak in temperatures at this time to produce a very low value of $\delta^{18}\text{O}_F$. This low value would be falsely interpreted (from figure 7b alone) as the strongest El Niño in the record. Large $\delta^{18}\text{O}_{sw}$ variability that is not related to ENSO can therefore interfere with the signal in archived $\delta^{18}\text{O}$, which is being used to understand ENSO. The reason that $\delta^{18}\text{O}_{sw}$ in this region is more variable in the mPWP than in the preindustrial is mainly because the hydrological cycle is stronger in the mPWP simulation [Bragg *et al.*, 2012; Haywood *et al.*, 2013]. Peak values of precipitation in this region are typically 40% larger in the mPWP and act to supply reduced $\delta^{18}\text{O}_p$ to the ocean, which in turn reduces $\delta^{18}\text{O}_{sw}$. In a month of large precipitation the $\delta^{18}\text{O}$ of the precipitation entering the ocean can be $\sim -10\text{‰}$ and can lower the $\delta^{18}\text{O}_{sw}$ from its typical value of $\sim 0.5\text{‰}$. The lowest value of $\delta^{18}\text{O}_{sw}$ ($\sim -0.8\text{‰}$) seen at months 16-17 in figure 8 corresponds to the largest precipitation value in this timeseries which has the lowest $\delta^{18}\text{O}_p$ value.

Although $\delta^{18}\text{O}_{sw}$ is clearly important for the surface ocean $\delta^{18}\text{O}_F$, at deeper levels its importance is diminished. This is because $\delta^{18}\text{O}_{sw}$ is less variable at deeper levels because precipitation and evaporation will have the largest effects near the ocean surface. Indeed at the 10-20m model level the variability in $\delta^{18}\text{O}_{sw}$ is typically half what it is at the 0-10m

model level. We noted previously that at the surface both $\delta^{18}\text{O}_{sw}$ and temperature were responsible for producing the unexpected low values of $\delta^{18}\text{O}_F$. The La Niña in months 16-17 appeared extraseasonal at the surface mainly because of the anomolous $\delta^{18}\text{O}_{sw}$, but this La Niña was also uncharacteristically warm in this gridbox. At deeper ocean levels, where the unexpected low $\delta^{18}\text{O}_F$ values in a La Niña month persist, $\delta^{18}\text{O}_{sw}$ varies less and temperature becomes relatively more important. Figure 8c shows temperature, $\delta^{18}\text{O}_{sw}$ and $\delta^{18}\text{O}_F$ for the final 50 years of the mPWP experiment from the 10-20m layer of the ocean. At 10-20m, unlike the surface layer, El Niño neither has warm temperatures or low $\delta^{18}\text{O}_F$ at this location. At this location, the highest temperatures and highest $\delta^{18}\text{O}_F$ do not represent El Niño, but instead represent either La Niña or neutral conditions, and the IFA method could not correctly attribute the low extraseasonal values of $\delta^{18}\text{O}_F$ to El Niño. The warm values that occur near this site during this La Niña episode (April year 2 in figure 8) is due to localised changes in ocean vertical velocity and do not reflect large scale conditions. Supplementary figure 6 shows the ocean vertical velocity for the surface layer of the ocean for the long term average preindustrial April conditions, long term average mPWP April conditions and the conditions that occurred in April year 2 on figure 8. In the model the location of this site (marked by the small box) is normally in a region of upwelling however there is a region of downwelling to the east of this region that is stronger in the mPWP than in the preindustrial. Small interannual shifts in this region of downwelling occur and can infrequently lead to high localised temperatures in the subsurface Eastern Pacific waters. This was the case in the month of very warm ocean temperatures (supplementary figure 6c) that was occurring as extraseasonal $\delta^{18}\text{O}_F$. In the final 300 years of the experiment there were 24 months with downwelling $> 1 \times 10^{-4} \text{cm s}^{-1}$

in the mPWP but only 2 months with downwelling $\dot{\lambda} 1 \times 10^{-4} \text{cm s}^{-1}$ in the preindustrial.

It is unclear whether this small region of downwelling in the mPWP simulation is reasonable or whether it is simply an artefact of the model, hence we do not state that this site is unsuitable for IFA analysis. However, this example highlights that it is possible for non-ENSO related features to affect a local site in the mPWP, but not in the modern, and this could make a method which appears suitable for ENSO detection based on modern data unsuitable for other time periods.

5.3. Which regions can ENSO be detected in IFA measurements?

In the same way that the model could simulate pseudo-corals from a large range of locations (see section 4.1), we can extend the planktonic foraminifera analysis to assess the IFA technique throughout the Pacific. We use the final 500 years of data from the simulation and simulate monthly individual foraminifera $\delta^{18}\text{O}_F$ measurements for the surface, for each gridbox across the Pacific.

Scropton et al. [2011] calculated that the probability of a month occurring with conditions that would be recorded as extraseasonal for *G. ruber*, the surface dwelling species, was 0.04. Following this we classify the lowest and highest 2% of simulated foram $\delta^{18}\text{O}_F$ as extraseasonal. According to IFA theory gridboxes which have high precipitation or warm temperatures in El Niño years are expected to simulate the lowest 2% of $\delta^{18}\text{O}_F$ values when there is an El Niño and the highest 2% of values when there is La Niña (see figure 1). Gridboxes which are dry in El Niño years are expected to simulate the highest 2% of $\delta^{18}\text{O}_F$ values when there is an El Niño and the lowest 2% of values when there is

La Niña (however as noted in the previous section this expectation may not always hold).

For each gridbox the fraction of extraseasonal events, which occur when the model is in the correct El Niño or La Niña state, is determined and results shown in figure 9, with only gridboxes where the extraseasonal events are correctly attributed in at least half of cases plotted. Note that the method of assessing pseudo-foraminifera is, by necessity, different to the ‘skill’ calculated from pseudo-coral in section 4.1. This is because a large number of true El Niño or La Niña months are not expected to be extraseasonal, and could not even theoretically be determined from an IFA. Unlike pseudo-coral analysis, the pseudo-foraminifera analysis is able to only consider whether extraseasonal events are being correctly attributed, and cannot make any assessment of the 96% of foraminifera that are not extraseasonal. Non-extraseasonal foraminifera could correctly represent any ENSO state.

As with the timeseries data (represented by coral; figure 5), results from planktonic foraminifera data (figure 9) are similar for the mPWP and the preindustrial. In general regions where a high fraction of extraseasonal values can be correctly attributed for the modern are also regions where extraseasonal events can be correctly attributed for the mPWP. However, as has been seen in the preceding sections, this is not the case for every ENSO event, and care must be taken when considering individual events from individual gridboxes. A single location can be subject to significant variability that is not related to ENSO, and without a continuous timeseries to analyse, short term variability can strongly affect a signal. Note that for the modeled continuous timeseries (represented by pseudocorals; figure 5) a single anomalous month is not able to incorrectly infer an

ENSO event, because the ONI definition requires an anomaly is to persist for 5 months, before an ENSO event will be inferred.

Figure 9 shows the extreme events incorrectly attributed to ENSO from the gridbox containing the *Scroxtton et al.* [2011] site are not typical for all ENSO events throughout the Pacific. Overall the fraction of extraseasonal values that are El Niño or La Niña is greater in the mPWP than it is for the preindustrial. In agreement with the pseudocorral data, the central Pacific is a particularly good region for ENSO detection, both for the mPWP and the preindustrial. The Western Pacific, where there is an increase in the ENSO precipitation signal, is the region that shows the greatest increase in skill in the mPWP. This is due to the fact that the ENSO related precipitation signal, is much stronger in the mPWP than in the preindustrial (see figure 1), while the ENSO related temperature change between the two climates is relatively smaller. It is also interesting that the region of highest skill differs between the two climates. The region where the IFA method appears to perform best is notably broader in the mPWP relative to the preindustrial.

5.4. Can ENSO amplitude changes be detected in IFA measurements?

The previous subsection considered which regions ENSO events could best be detected in IFA measurements for the mPWP and the preindustrial. We now turn our attention to whether it is possible to detect changes in ENSO amplitude between the mPWP and preindustrial. If so, this could resolve conflicts between modeling studies as to whether ENSO was stronger or weaker in the mPWP [*Tindall et al.*, 2016; *Brierley*, 2015]. We

use the INFAUNAL forward model, [Thirumalai et al., 2013, 2014], which considers IFA statistics from multiple samples of a population, to determine whether ENSO changes between the preindustrial and the mPWP climates can be detected. INFAUNAL is briefly described here: firstly, for a given site, INFAUNAL calculates the foram $\delta^{18}\text{O}_F$ for the climatological annual cycle and for a climatologically averaged El Niño and La Niña event (based on the 2σ threshold of SSTs in the Niño3.4 box). Next, it takes a foram $\delta^{18}\text{O}_F$ population representing a time interval (e.g. 500 years) and will sample a number (n) of individual forams. The original population is then statistically altered by increasing or decreasing the strength of the annual cycle and/or the strength of ENSO, and a random sample of n individuals from the altered population taken. Finally, INFAUNAL statistically compares the sample from the original population, with the sample from the altered population. Doing this many times allows INFAUNAL to calculate the probability of detecting a significant change in population statistics, due to either changes in the annual cycle or ENSO. It accounts for both sampling error and the difficulty in disentangling the signal of the annual cycle from the interannual variability.

INFAUNAL is used here in a novel way to assess the likely ability of *G. ruber*-based IFA measurements to resolve ENSO changes between our preindustrial and mPWP simulations. *G. ruber* is a specie that can thrive throughout the year and IFA statistics will therefore be sensitive to the ratio of annual cycle variability to ENSO variability within each time interval [Thirumalai et al., 2013]. We first selected a site from the preindustrial simulation and a site from the mPWP simulation that figure 9 suggests have particularly high skill in accurately categorising ENSO events for each climate. The preindustrial site

used is at 8.125°S, 141.25°W, and the mPWP site used is at 0.625°N, 162.5°W and they will be hereafter referred to as PreindMax and PlioMax respectively. We assume that the final 500 years of model output represents the population that would be sampled in a 500 year resolution of sediment [Thirumalai *et al.*, 2013], and consider how many samples are needed to accurately represent the population statistics. Figures 10(a) and (c) show that as the number of samples increase both accuracy (defined as the error in sample standard deviation) and precision (defined as the estimated spread of sample standard deviation) improves and that 50 IFA measurements are sufficient for providing a reasonable estimate of population standard deviation at these sites (for 50 samples the error in sample standard deviation is usually < 0.05). We then took multiple random samples of 50 foraminifera from both the original population and altered populations (with different magnitudes of both the annual cycle and ENSO) to calculate the probability of detecting a change in ENSO/annual cycle statistics in sampled foraminifera. Ultimately, the ratio of interannual-to-annual variability at these sites determines whether a change in sample statistics is likely due to annual cycle or ENSO changes.

In the preindustrial simulation, the ENSO amplitude of $\delta^{18}\text{O}_F$ is similar at both the PreindMax and PlioMax sites (0.28‰; figure 11). The annual cycle at the PreindMax site is smaller than at the PlioMax site (0.17‰ compared to 0.28‰), showing that for the preindustrial simulation there is a higher interannual-to-annual ratio at the PreindMax site compared to the PlioMax site. This suggests that, considering the preindustrial simulation alone, the PreindMax site is a better location for detecting ENSO changes than

the PlioMax site.

In the mPWP simulation, the sites show an increase in ENSO amplitude but a larger increase in annual cycle amplitude, such that the interannual-to-annual ratio is reduced in the mPWP, particularly at the PlioMax site. Consequently, we generate two INFAUNAL probability contour diagrams with the following original populations: 1) the preindustrial simulation at the PreindMax site (figure 10b) with the yellow star at [0,0] representing the unaltered preindustrial population 2) the mPWP simulation at the PlioMax site (figure 10d) with the yellow star at [0,0] representing the unaltered mPWP population.

Figure 10b shows that at the PreindMax site a change from preindustrial IFA sample (yellow star) to a mPWP IFA sample (red circle) is unlikely ($< 10\%$ probability) to produce significantly different sample statistics. Although INFAUNAL generates probability contours at the PreindMax site that are sensitive to ENSO rather than the annual cycle, at this location there is very little change in the strength of ENSO between the climates and the small change is unlikely to be detected with IFA. At the PlioMax site the results are different. The annual cycle is relatively stronger here and the probability contours are therefore more skewed. However at this location the difference between samples from the mPWP simulation (yellow star) and the preindustrial simulation (red circle) shows an increased likelihood (40% probability) of being detected in sampled statistics, although some of this increased probability is due to the increased strength of the annual cycle.

In summary, there are two necessary constraints for choosing an optimal location to perform IFA to detect changes in ENSO: 1) a site should have a sufficiently high ratio of

interannual-to-annual variability to begin with (e.g. PreindMax) and 2) there is a sufficiently large change during the altered climate state (e.g PlioMax). Thus, this exercise demonstrates the utility of paleosimulation in providing direction for choosing optimal sampling locations as an apparently ideal site based on the the preindustrial/modern climate (e.g. figure 10b) can have lower skill for detecting paleoclimate changes than sites which initially appear less ideal (e.g. figure 10d).

6. Conclusions

This paper has used model simulations of the mPWP and the preindustrial to directly simulate paleoproxy data throughout the Pacific. The simulated paleoproxy data has been compared with the modeled Oceanic Nino Index in order to determine the theoretical locations where proxy data could accurately represent mPWP ENSO signatures.

The first type of data considered was HadCM3 derived ‘pseudo-corals’ which were intended to represent archives where a continuous time series with high temporal resolution could be available, such as coral or Mollusk data. For completeness a pseudo-coral was produced for each gridbox in the tropical Pacific, even though the potential for such data to exist is limited to a small number of localities. Looking at individual localities where a strong ENSO signal was expected, it was found that the skill of accurately detecting ENSO was slightly larger in the mPWP than in the preindustrial (due to the stronger El Niño signal in the mPWP). However this slight increase in skill between the two time periods was minor when compared with the large variation in skill due to location.

In general, areas which have a good skill at ENSO detection in the preindustrial also

have good skill in the mPWP. The reasoning of *Watanabe et al.* [2011], which compared mPWP coral with a nearby live coral, to assess ENSO behavior is supported by our study.

HadCM3 was also used to derive bulk and individual ‘pseudo-foraminifera’. The bulk pseudo-foraminifera was used to assess the east-west gradient across the Pacific [*Wara et al.*, 2005] with the aim of interpreting data which indicates a ‘permanent El Niño’. Although the data shows reduced temperature and $\delta^{18}\text{O}_F$ gradients across the tropical Pacific in the Pliocene this could not be reproduced with the model simulation representing 3.2Ma. However, our analysis highlighted that both temperature and $\delta^{18}\text{O}_F$ were subject to large spatial gradients in these regions and suggested that a shift in climate zones could explain the data without the requirement of a permanent El Niño.

Pseudo-foraminifera were used to assess the ability of Individual Foraminifera Analysis (IFA) to detect El Niño. A case study of a location in the Eastern Equatorial Pacific found that El Niño could be detected in IFA from the preindustrial simulation but not from the mPWP simulation. However, we acknowledge the limitations of considering model output from a single model gridbox, and do not claim that any location should necessarily be avoided for ENSO studies. Instead we highlight that there could be different processes occurring in a different climate and that validating the IFA method using modern data may not mean that this method is suitable for other periods. This is in contrast to what we suggested for timeseries data (such as coral), as in timeseries data a non-ENSO anomaly would have to persist for several months to affect the results.

Despite the mPWP simulation suggesting that the IFA technique could be unreliable at some locations, results based on this method were generally encouraging. Across most of the Pacific this technique had greater skill in accurately attributing extraseasonal events to El Niño and La Niña conditions for the mPWP than for the preindustrial. In the central and western central Pacific the skill was particularly improved.

Site location was also shown to be important for detecting possible changes in El Niño amplitude between the mPWP and the preindustrial. A site which appeared ideal, based on preindustrial ENSO statistics, had extremely low probability of detecting changes between the climates. The probability of detecting a change between the two climates was much higher at a site which initially appeared less ideal from the preindustrial perspective.

Throughout this paper the central Pacific has been highlighted as one region where paleoproxies are likely to provide a good signal of ENSO variability. Data which has a continuous time series (like corals) and data which has high resolution but is not continuous (like individual foraminifera) both perform well in this region. The model suggests that if data from this region provides an indication of ENSO activity, there is good confidence that El Niño, La Niña and neutral conditions are correctly attributed.

In our simulations the mPWP hydrological cycle was enhanced, and non ENSO related precipitation was also enhanced. The implications of this are twofold. Firstly, in a region that is influenced by ENSO, but with little other variability, ENSO should be easier to detect than in the modern. Secondly, non-ENSO related variability could be stronger in

the mPWP climate and this may mask the ENSO signal in mPWP data even if it does not in the modern. This highlights the importance of considering all periods of variability when interpreting proxy data from a single site.

Acknowledgments. Research leading to these results has received funding from the European Research Council under the European Union's Seventh Framework Programme (FP7/2007-2013)/ERC grant agreement no. 278636, and KT acknowledges funding from UTIG. The authors would like to thank Tsuyoshi Watanabe for providing the coral data used to produce figure 2, Steven Pickering for modeling support and two anonymous reviewers for helpful comments which have greatly improved the manuscript. Model data used to produce figures 1-9 is attached as supporting information, data used to produce figures 10 and 11 can be obtained from KT.

References

- AchutaRao, K., and K. R. Sperber (2002), Simulation of the El Nino Southern Oscillation: Results from the Coupled Model Intercomparison Project, *Clim. Dyn.*, *19*(3-4), 191–209.
- Bellenger, H., E. Guilyardi, J. Leloup, M. Lengaigne, and J. Vialard (2014), ENSO representation in climate models: from CMIP3 to CMIP5, *Clim. Dyn.*, *42*(7-8), 1999–2018, doi:10.1007/s00382-013-1783-z.
- Bonham, S. G., A. M. Haywood, D. J. Lunt, M. Collins, and U. Salzmann (2009), El Nino-Southern Oscillation, Pliocene climate and equifinality, *PHILOSOPHICAL TRANSACTIONS OF THE ROYAL SOCIETY A-MATHEMATICAL PHYSICAL AND ENGINEERING Sciences*, *367*(1886), 127–156, doi:10.1098/rsta.2008.0212.
- Bragg, F. J., D. J. Lunt, and A. M. Haywood (2012), Mid-Pliocene climate modelled using the UK Hadley Centre Model: PlioMIP Experiments 1 and 2, *Geosci. Model Dev.*, *5*(5), 1109–1125, doi:10.5194/gmd-5-1109-2012.
- Brierley, C. M. (2015), Interannual climate variability seen in the Pliocene Model Intercomparison Project, *Climate of the Past*, *11*(3), 605–618.
- Collins, M., S.-I. An, W. Cai, A. Ganachaud, E. Guilyardi, F.-F. Jin, M. Jochum, M. Lengaigne, S. Power, A. Timmermann, G. Vecchi, and A. Wittenberg (2010), The impact of global warming on the tropical Pacific ocean and El Nino, *Nature Geoscience*, *3*(6), 391–397, doi:10.1038/NGEO868.
- Cox, P., R. A. Betts, C. B. Bunton, R. L. H. Essery, P. R. Rowntree, and J. Smith (1999), The impact of new land surface physics on the GCM simulation of climate and climate sensitivity, *Clim. Dyn.*, *15*(3), 183–203.

Dai, A. (2006), Precipitation characteristics in eighteen coupled climate models, *Journal of Climate*, *19*(18), 4605–4630, doi:10.1175/JCLI3884.1.

Dai, A., and T. M. L. Wigley (2000), Global patterns of ENSO-induced precipitation, *Geophys. Res. Lett.*, *27*(9), 1283–1286.

Dee, S., D. Noone, N. Buening, J. Emile-Geay, and Y. Zhou (2015), SPEEDY-IER: A fast atmospheric GCM with water isotope physics, *JOURNAL OF GEOPHYSICAL RESEARCH-ATMOSPHERES*, *120*(1), 73–91, doi:10.1002/2014JD022194.

Dekens, P., D. Lea, D. Pak, and H. Spero (2002), Core top calibration of Mg/Ca in tropical foraminifera: Refining paleotemperature estimation, *GEOCHEMISTRY GEOPHYSICS GEOSYSTEMS*, *3*, doi:10.1029/2001GC000200.

Dolan, A. M., A. M. Haywood, D. J. Hill, H. J. Dowsett, S. J. Hunter, D. J. Lunt, and S. J. Pickering (2011), Sensitivity of Pliocene ice sheets to orbital forcing, *Palaeogeogr. Palaeoclimatol. Palaeoecol.*, *309*(1-2), 98–110.

Dowsett, H., M. Robinson, A. Haywood, U. Salzmann, D. Hill, L. Sohl, M. Chandler, M. Williams, K. Foley, and D. Stoll (2010), The PRISM3D paleoenvironmental reconstruction, *Stratigraphy*, *7*(2-3), 123–139.

Dowsett, H., A. Dolan, D. Rowley, R. Moucha, A. M. Forte, J. X. Mitrovica, M. Pound, U. Salzmann, M. Robinson, M. Chandler, K. Foley, and A. Haywood (2016), The PRISM4 (mid-Piacenzian) paleoenvironmental reconstruction, *Climate of the Past*, *12*(7), 1519–1538, doi:10.5194/cp-12-1519-2016.

Edwards, J. M., and A. Slingo (1996), Studies with a flexible new radiation code. 1. Choosing a configuration for a large-scale model, *Q. J. R. Meteorol. Soc.*, *122*(531), 689–719.

Erez, J., and B. Luz (1983), Experimental paleotemperature equation for planktonic-foraminifera, *Geochim. Cosmochim. Acta.*, *47*(6), 1025–1031.

Fedorov, A., P. Dekens, M. McCarthy, A. Ravelo, P. deMenocal, M. Barreiro, R. Pacanowski, and S. Philander (2006), The Pliocene paradox (mechanisms for a permanent El Nino), *Science*, *312*(5779), 1485–1489, doi:10.1126/science.1122666.

Goddard, L., and M. Dille (2005), El Nino: Catastrophe or opportunity, *JOURNAL OF CLIMATE*, *18*(5), 651–665, doi:10.1175/JCLI-3277.1.

Gordon, C., C. Cooper, C. Senior, H. Banks, J. Gregory, T. Johns, J. Mitchell, and R. Wood (2000), The simulation of SST, sea ice extents and ocean heat transports in a version of the Hadley Centre coupled model without flux adjustments, *Clim. Dyn.*, *16*(2-3), 147–168.

Gregory, D., and D. Morris (1996), The sensitivity of climate simulations to the specification of mixed phase clouds, *Clim. Dyn.*, *12*(9), 641–651.

Gregory, D., and P. R. Rowntree (1990), A mass flux convection scheme with representation of cloud ensemble characteristics and stability-dependent closure, *Mon. Weather Rev.*, *118*(7), 1483–1506.

Guilyardi, E. (2006), El Nino-mean state-seasonal cycle interactions in a multi-model ensemble, *Climate Dynamics*, *26*(4), 329–348, doi:10.1007/s00382-005-0084-6.

Haese, B., M. Werner, and G. Lohmann (2013), Stable water isotopes in the coupled atmosphere-land surface model ECHAM5-JSBACH, *GEOSCIENTIFIC MODEL DEVELOPMENT*, *6*(5), 1463–1480, doi:10.5194/gmd-6-1463-2013.

Haywood, A. M., P. J. Valdes, and B. W. Sellwood (2000), Global scale palaeoclimate reconstruction of the middle Pliocene climate using the UKMO GCM: initial results,

Glob. Planet. Chang., 25(3-4), 239–256.

Haywood, A. M., H. J. Dowsett, B. Otto-Bliesner, M. A. Chandler, A. M. Dolan, D. J.

Hill, D. J. Lunt, M. M. Robinson, N. Rosenbloom, U. Salzmann, and L. E. Sohl (2010),

Pliocene Model Intercomparison Project (PlioMIP): experimental design and boundary conditions (Experiment 1), *Geosci. Model Dev.*, 3(1), 227–242.

Haywood, A. M., H. J. Dowsett, M. M. Robinson, D. K. Stoll, A. M. Dolan, D. J. Lunt,

B. Otto-Bliesner, and M. A. Chandler (2011), Pliocene Model Intercomparison Project (PlioMIP): experimental design and boundary conditions (Experiment 2), *Geosci. Model Dev.*, 4(3), 571–577.

Haywood, A. M., D. J. Hill, A. M. Dolan, B. L. Otto-Bliesner, F. Bragg, W. L. Chan,

M. A. Chandler, C. Contoux, H. J. Dowsett, A. Jost, Y. Kamae, G. Lohmann, D. J.

Lunt, A. Abe-Ouchi, S. J. Pickering, G. Ramstein, N. A. Rosenbloom, U. Salzmann,

L. Sohl, C. Stepanek, H. Ueda, Q. Yan, and Z. Zhang (2013), Large-scale features of Pliocene climate: results from the Pliocene Model Intercomparison Project, *Clim. Past*, 9(1), 191–209.

Haywood, A. M., P. J. Valdes, and V. L. Peck (2007), A permanent El Niño-like state

during the Pliocene?, *Paleoceanography*, 22(1), doi:10.1029/2006PA001323.

Haywood, A. M., A. M. Dolan, S. J. Pickering, H. J. Dowsett, E. L. McClymont, C. L.

Prescott, U. Salzmann, D. J. Hill, S. J. Hunter, D. J. Lunt, J. O. Pope, and P. J. Valdes

(2013), On the identification of a Pliocene time slice for data-model comparison, *Philos. T. Roy. Soc. A*, 371(2001), doi:10.1098/rsta.2012.0515.

Haywood, A. M., H. J. Dowsett, and A. M. Dolan (2016), Integrating geological archives

and climate models for the mid-Pliocene warm period, *NATURE COMMUNICATIONS*,

Hereid, K. A., T. M. Quinn, and Y. M. Okumura (2013), Assessing spatial variability in El Nino-Southern Oscillation event detection skill using coral geochemistry, *PALEOCEANOGRAPHY*, *28*(1), doi:10.1029/2012PA002352.

Hill, D. J. (2015), The non-analogue nature of Pliocene temperature gradients, *EARTH AND PLANETARY SCIENCE LETTERS*, *425*, 232–241, doi:10.1016/j.epsl.2015.05.044.

Holmes, J. A., J. Tindall, N. Roberts, W. Marshall, J. D. Marshall, A. Bingham, I. Feeser, M. O’Connell, T. Atkinson, A.-L. Jourdan, A. March, and E. H. Fisher (2016), Lake isotope records of the 8200-year cooling event in western Ireland: Comparison with model simulations, *QUATERNARY SCIENCE REVIEWS*, *131*(B), 341–349, doi:10.1016/j.quascirev.2015.06.027.

Juillet-Leclerc, A., and G. Schmidt (2001), A calibration of the oxygen isotope paleothermometer of coral aragonite from Porites, *Geophys. Res. Lett.*, *28*(21), 4135–4138.

Koutavas, A., P. B. deMenocal, G. C. Olive, and J. Lynch-Stieglitz (2006), Mid-Holocene El Nino-Southern Oscillation (ENSO) attenuation revealed by individual foraminifera in eastern tropical Pacific sediments, *GEOLOGY*, *34*(12), 993–996, doi:10.1130/G22810A.1.

Latif, M., and N. S. Keenlyside (2009), El Nino/Southern Oscillation response to global warming, *PROCEEDINGS OF THE NATIONAL ACADEMY OF SCIENCES OF THE UNITED STATES OF AMERICA*, *106*(49), 20,578–20,583, doi:10.1073/pnas.0710860105.

- Lee, J.-E., I. Fung, D. J. DePaolo, and C. C. Henning (2007), Analysis of the global distribution of water isotopes using the NCAR atmospheric general circulation model, *J. Geophys. Res-Atmos.*, *112*(D16), doi:10.1029/2006JD007657.
- Li, J., S.-P. Xie, E. R. Cook, G. Huang, R. D'Arrigo, F. Liu, J. Ma, and X.-T. Zheng (2011), Interdecadal modulation of El Nino amplitude during the past millennium, *Nature Climate Change*, *1*(2), 114–118, doi:10.1038/NCLIMATE1086.
- McGregor, S., A. Timmermann, and O. Timm (2010), A unified proxy for ENSO and PDO variability since 1650, *CLIMATE OF THE PAST*, *6*(1), 1–17.
- Miller, K. G., J. D. Wright, J. V. Browning, A. Kulpecz, M. Kominz, T. R. Naish, B. S. Cramer, Y. Rosenthal, W. R. Peltier, and S. Sosdian (2012), High tide of the warm Pliocene: Implications of global sea level for Antarctic deglaciation, *Geology*, *40*(5), 407–410.
- Molnar, P., and M. Cane (2002), El Nino's tropical climate and teleconnections as a blueprint for pre-Ice Age climates, *Paleoceanography*, *17*(2), doi:10.1029/2001PA000663.
- Philander, S., and A. Fedorov (2003), Role of tropics in changing the response to Milankovich forcing some three million years ago, *Paleoceanography*, *18*(2), doi:10.1029/2002PA000837.
- Pope, V., M. Gallani, P. Rowntree, and R. Stratton (2000), The impact of new physical parametrizations in the Hadley Centre climate model: HadAM3, *Clim. Dyn.*, *16*(2-3), 123–146.
- Pound, M. J., J. Tindall, S. J. Pickering, A. M. Haywood, H. J. Dowsett, and U. Salzmann (2014), Late Pliocene lakes and soils: a global data set for the analysis of climate feedbacks in a warmer world, *Clim. Past*, *10*(1), 167–180, doi:10.5194/cp-10-167-2014.

- Prescott, C. L., A. M. Haywood, A. M. Dolan, S. J. Hunter, J. O. Pope, and S. J. Pickering (2014), Assessing orbitally-forced interglacial climate variability during the mid-Pliocene Warm Period, *Earth. Planet. Sci. Lett.*, *400*, 261–271.
- Ravelo, A. C., K. T. Lawrence, A. Fedorov, and H. L. Ford (2014), Comment on “A 12-million-year temperature history of the tropical Pacific Ocean”, *SCIENCE*, *346*(6216), doi:10.1126/science.1257618.
- Roberts, C. D., A. N. LeGrande, and A. K. Tripathi (2011), Sensitivity of seawater oxygen isotopes to climatic and tectonic boundary conditions in an early Paleogene simulation with GISS ModelE-R, *Paleoceanography*, *26*, doi:10.1029/2010PA002025.
- Roche, D. M. (2013), delta O-18 water isotope in the iLOVECLIM model (version 1.0) - Part 1: Implementation and verification, *GEOSCIENTIFIC MODEL DEVELOPMENT*, *6*(5), 1481–1491, doi:10.5194/gmd-6-1481-2013.
- Salzmann, U., A. M. Dolan, A. M. Haywood, W. L. Chan, J. Voss, D. J. Hill, A. Abe-Ouchi, B. Otto-Bliesner, F. J. Bragg, M. A. Chandler, C. Contoux, H. J. Dowsett, A. Jost, Y. Kamae, G. Lohmann, D. J. Lunt, S. J. Pickering, M. J. Pound, G. Ramstein, N. A. Rosenbloom, L. Sohl, C. Stepanek, H. Ueda, and Z. S. Zhang (2013), Challenges in quantifying Pliocene terrestrial warming revealed by data-model discord, *Nat. Clim. Chang.*, *3*(11), 969–974.
- Scroxton, N., S. Bonham, R. E. M. Rickaby, S. H. F. Lawrence, M. Hermoso, and A. M. Haywood (2011), Persistent El Nino-Southern Oscillation variation during the Pliocene Epoch, *Paleoceanography*, *26*.
- Seki, O., G. L. Foster, D. N. Schmidt, A. Mackensen, K. Kawamura, and R. D. Pancost (2010), Alkenone and boron-based Pliocene pCO(2) records, *Earth and Planetary*

Science Letters, 292(1-2), 201–211, doi:10.1016/j.epsl.2010.01.037.

Seki, O., D. N. Schmidt, S. Schouten, E. C. Hopmans, J. S. S. Damste, and R. D. Pancost (2012), Paleooceanographic changes in the Eastern Equatorial Pacific over the last 10

Myr, *Paleoceanography*, 27, doi:10.1029/2011PA002158.

Semtner, A. J. (1976), Model for thermodynamic growth of sea ice in numerical investigations of climate, *J. Phys. Oceanogr.*, 6(3), 379–389.

Smith, R. N. B. (1990), A scheme for predicting layer clouds and their water-content in a general-circulation model, *Q. J. R. Meteorol. Soc.*, 116(492), 435–460.

Stap, L. B., B. de Boer, M. Ziegler, R. Bintanja, L. J. Lourens, and R. S. W. van de Wal (2016), CO₂ over the past 5 million years: Continuous simulation and new delta B-11-based proxy data, *EARTH AND PLANETARY SCIENCE LETTERS*, 439, 1–10, doi:10.1016/j.epsl.2016.01.022.

Steph, S., R. Tiedemann, M. Prange, J. Groeneveld, M. Schulz, A. Timmermann, D. Nuernberg, C. Ruehlemann, C. Saukel, and G. H. Haug (2010), Early Pliocene increase in thermohaline overturning: A precondition for the development of the modern equatorial Pacific cold tongue, *PALEOCEANOGRAPHY*, 25, doi:10.1029/2008PA001645.

Stevenson, S., B. S. Powell, M. A. Merrifield, K. M. Cobb, J. Nusbaumer, and D. Noone (2015), Characterizing seawater oxygen isotopic variability in a regional ocean modeling framework: Implications for coral proxy records, *PALEOCEANOGRAPHY*, 30(11), 1573–1593, doi:10.1002/2015PA002824.

Thirumalai, K., J. W. Partin, C. S. Jackson, and T. M. Quinn (2013), Statistical constraints on El Niño Southern Oscillation reconstructions using individual

foraminifera: A sensitivity analysis, *PALEOCEANOGRAPHY*, *28*(3), 401–412, doi:10.1002/palo.20037.

Thirumalai, K., J. N. Richey, T. M. Quinn, and R. Z. Poore (2014), Globigerinoides ruber morphotypes in the Gulf of Mexico: A test of null hypothesis, *SCIENTIFIC REPORTS*, *4*, doi:10.1038/srep06018.

Tindall, J., R. Flecker, P. Valdes, D. N. Schmidt, P. Markwick, and J. Harris (2010), Modelling the oxygen isotope distribution of ancient seawater using a coupled ocean-atmosphere GCM: Implications for reconstructing early Eocene climate, *Earth. Planet. Sci. Lett.*, *292*(3-4), 265–273, doi:10.1016/j.epsl.2009.12.049.

Tindall, J. C., and A. M. Haywood (2015), Modeling oxygen isotopes in the Pliocene: Large-scale features over the land and ocean, *PALEOCEANOGRAPHY*, *30*(9), 1183–1201, doi:10.1002/2014PA002774.

Tindall, J. C., P. J. Valdes, and L. C. Sime (2009), Stable water isotopes in HadCM3: Isotopic signature of El Nino Southern Oscillation and the tropical amount effect, *J. Geophys. Res-Atmos.*, *114*, doi:10.1029/2008JD010825.

Tindall, J. C., A. M. Haywood, and F. W. Howell (2016), Accounting for Centennial Scale variability when Detecting Changes in ENSO: A study of the Pliocene, *Paleoceanography*, doi:10.1002/2016PA002951.

von der Heydt, A. S., A. Nnafie, and H. A. Dijkstra (2011), Cold tongue/Warm pool and ENSO dynamics in the Pliocene, *Climate of the Past*, *7*(3), 903–915, doi:10.5194/cp-7-903-2011.

Wang, H., R. Zhang, J. Cole, and F. Chavez (1999), El Nino and the related phenomenon Southern Oscillation (ENSO): The largest signal in interannual climate variation, *PRO-*

- Wara, M., A. Ravelo, and M. Delaney (2005), Permanent El Nino-like conditions during the Pliocene warm period, *Science*, 309(5735), 758–761, doi:10.1126/science.1112596.
- Watanabe, T., A. Suzuki, S. Minobe, T. Kawashima, K. Kameo, K. Minoshima, Y. M. Aguilar, R. Wani, H. Kawahata, K. Sowa, T. Nagai, and T. Kase (2011), Permanent El Nino during the Pliocene warm period not supported by coral evidence, *Nature*, 471(7337), 209–211.
- Winnick, M. J., J. M. Welker, and C. P. Chamberlain (2013), Stable isotopic evidence of El Nino-like atmospheric circulation in the Pliocene western United States, *Clim. Past*, 9(5), 2085–2099.
- Wittenberg, A. T. (2009), Are historical records sufficient to constrain ENSO simulations?, *Geophysical Research Letters*, 36, doi:10.1029/2009GL038710.
- Zhang, Y. G., M. Pagani, and Z. Liu (2014a), A 12-Million-Year Temperature History of the Tropical Pacific Ocean, *Science*, 344(6179), 84–87, doi:10.1126/science.1246172.
- Zhang, Y. G., M. Pagani, and Z. Liu (2014b), Response to Comment on “A 12-million-year temperature history of the tropical Pacific Ocean”, *SCIENCE*, 346(6216), doi:10.1126/science.1257930.
- Zhang, Z., Q. Yan, J. Z. Su, and Y. Q. Gao (2012), Has the Problem of a Permanent El Nio been Resolved for the Mid-Pliocene?, *Atmospheric and Oceanic Science Letters*, 5(6), 445–448, doi:10.1080/16742834.2012.11447035.

mPWP				
Location	Phase	Detected (as %age of modeled events)	Not detected (as %age of modeled events)	False positive (as %age of predicted events)
a) 0N, 190E	El Niño	41 (95%)	2 (5%)	6 (13%)
Central Pacific	La Niña	53 (98%)	1 (2%)	18 (25%)
b) 6.875S, 278.75E	El Niño	41 (95%)	2 (5%)	19 (32%)
Eastern Pacific	La Niña	48 (89%)	6 (11%)	24 (33%)
c) 3.125S, 141.25E	El Niño	37 (86%)	6 (14%)	22 (37%)
-ve $\delta^{18}O_{sw}$ signal	La Niña	39 (72%)	15 (28%)	21 (35%)
d) 15S, 175E	El Niño	38 (88%)	5 (12%)	23 (38%)
+ve $\delta^{18}O_{sw}$ signal	La Niña	45 (83%)	9 (17%)	31 (41%)
total across all phases and locations		342 (88%)	46 (12%)	164 (32%)

preindustrial				
Location	Phase	Detected	Not detected	False positive
a) 0N, 190E	El Niño	51 (100%)	0 (0%)	18 (26%)
Central Pacific	La Niña	49 (98%)	1 (2%)	19 (27%)
b) 6.875S, 278.75E	El Niño	44 (86%)	7 (14%)	25 (36%)
Eastern Pacific	La Niña	36 (72%)	14 (28%)	35 (49%)
c) 3.125S, 141.25E	El Niño	38 (75%)	13 (25%)	35 (48%)
-ve $\delta^{18}O_{sw}$ signal	La Niña	34 (68%)	16 (32%)	45 (57%)
d) 15S, 175E	El Niño	40 (78%)	11 (22%)	24 (37%)
+ve $\delta^{18}O_{sw}$ signal	La Niña	37 (74%)	13 (26%)	47 (56%)
total across all phases and locations		329 (81%)	75 (19%)	248 (42%)

Table 1. Ability to detect El Niño and La Niña in model produced pseudo-coral $\delta^{18}O_c$ at a single location. Results are from the final 300 years of the mPWP and the preindustrial simulations.

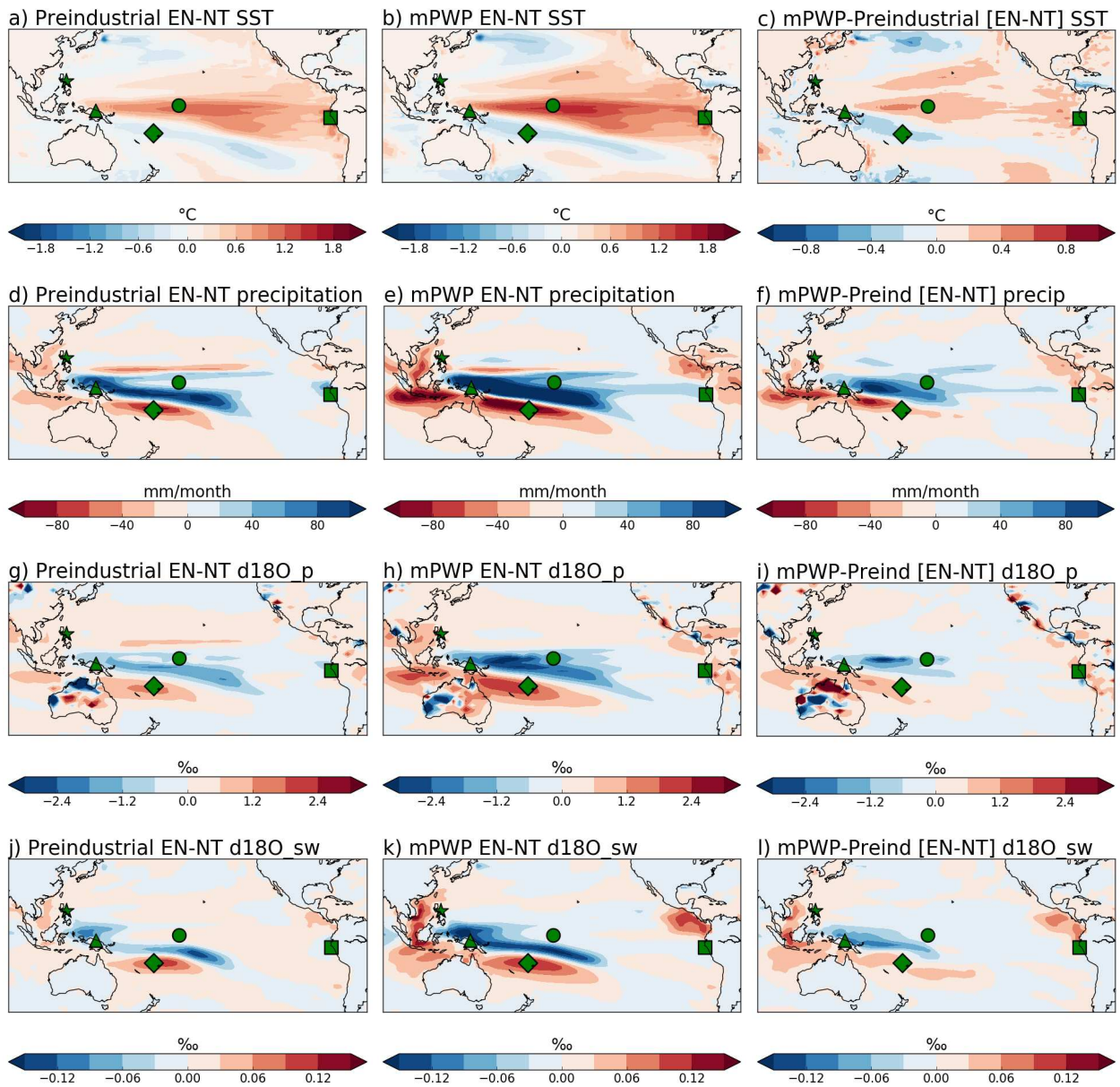


Figure 1. Anomalies between El Niño (EN) and neutral (NT) climate states for the preindustrial (left), mPWP (center) and the difference between them (mPWP EN-NT anomalies minus preindustrial EN-NT anomalies; right). Sites discussed in section 4 are shown as: a) 0°N, 190°E - circle, b) 7°S, 81°W - square, c) 3°S, 141°E - triangle d) 16°S, 175°E - diamond. The location of the coral data of *Watanabe et al.* [2011] is marked by the star.

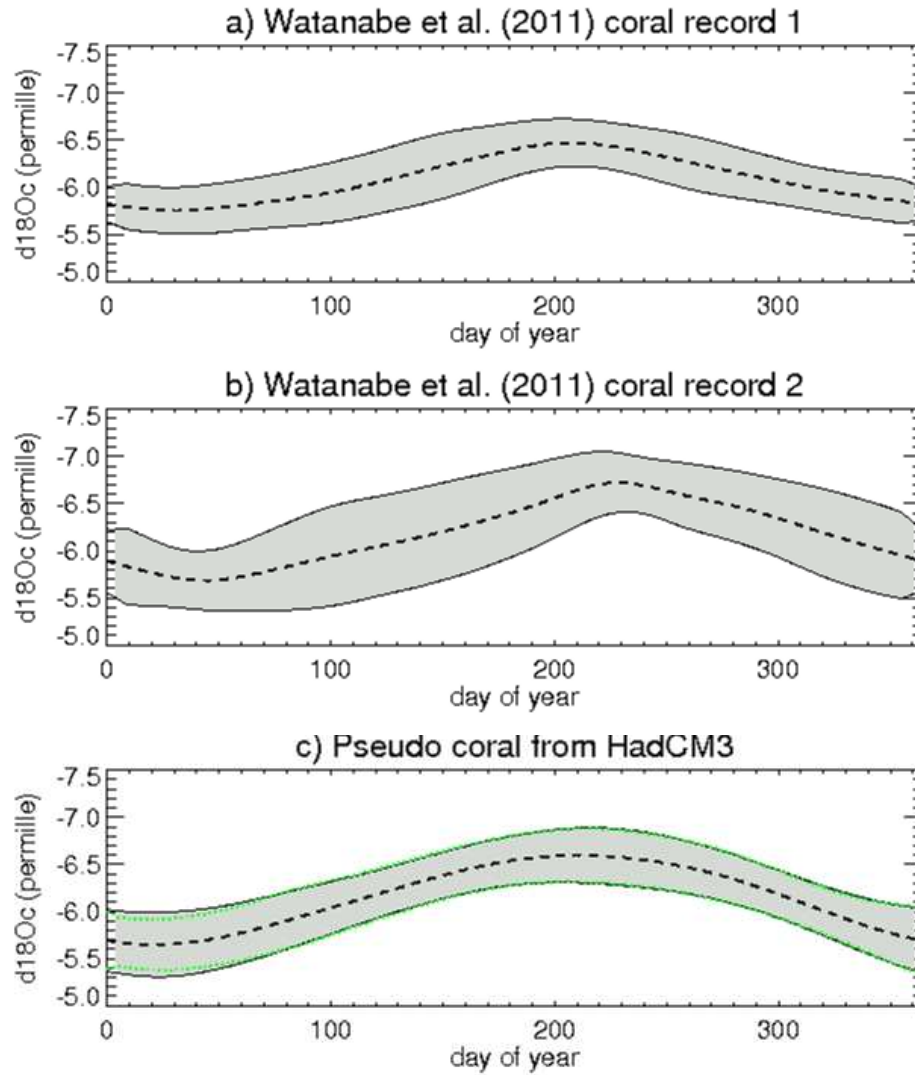


Figure 2. Coral data from *Watanabe et al.* [2011] and pseudo coral $\delta^{18}\text{O}_c$ obtained from HadCM3. Shown is the mean annual cycle (dashed line) and the mean annual cycle ± 2 standard deviations (shaded region). The shaded region corresponds to approximate 95% confidence interval on the mean. In figure 2c the the black (green) line encloses the mean ± 2 standard deviations region as calculated from the last 35 (300) years of model simulation.

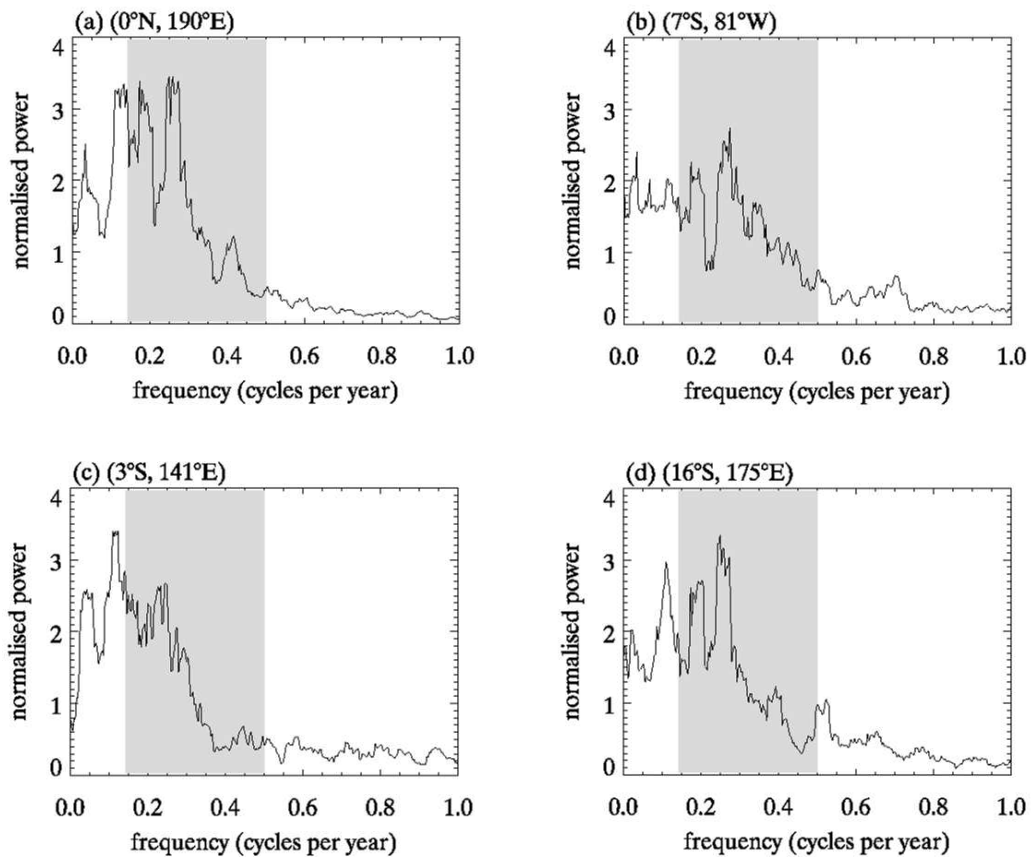


Figure 3. Power spectral density from a modeled 300 year coral from each of the 4 sites (a-d) in the caption of figure 1. The shaded band highlights frequencies corresponding to the expected 2-7 year period of ENSO. The power has been normalised by dividing by the variance of the coral and the frequency resolution. A 10 point running mean is presented for clarity.

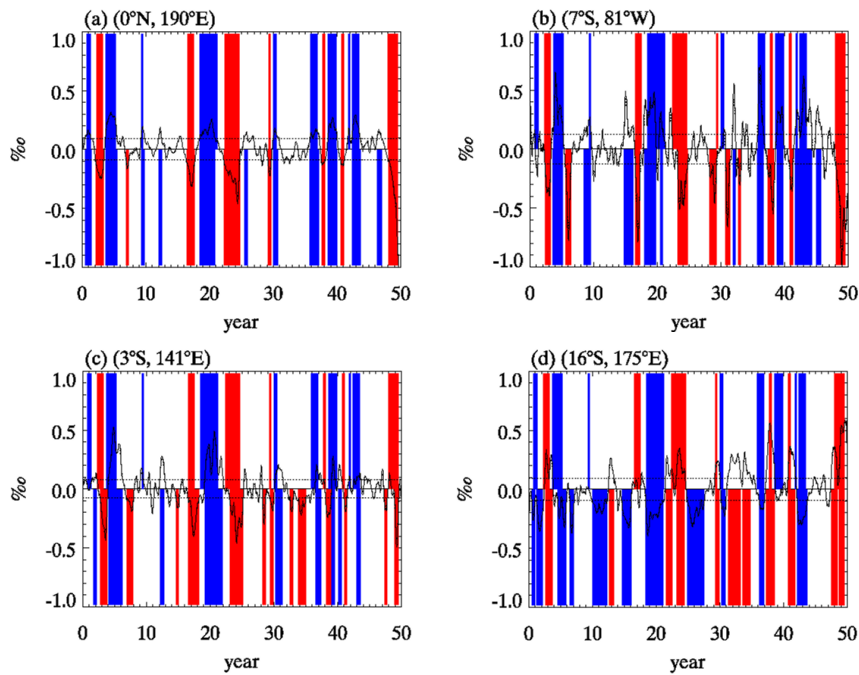


Figure 4. Modeled coral at the 4 locations (a-d) shown in figure 1. Bands above the x-axis show times where El Niño (red) and La Niña (blue) were present in the simulation. Bands below the axis show times when El Niño (red) and La Niña (blue) were inferred from the pseudo coral at the location.

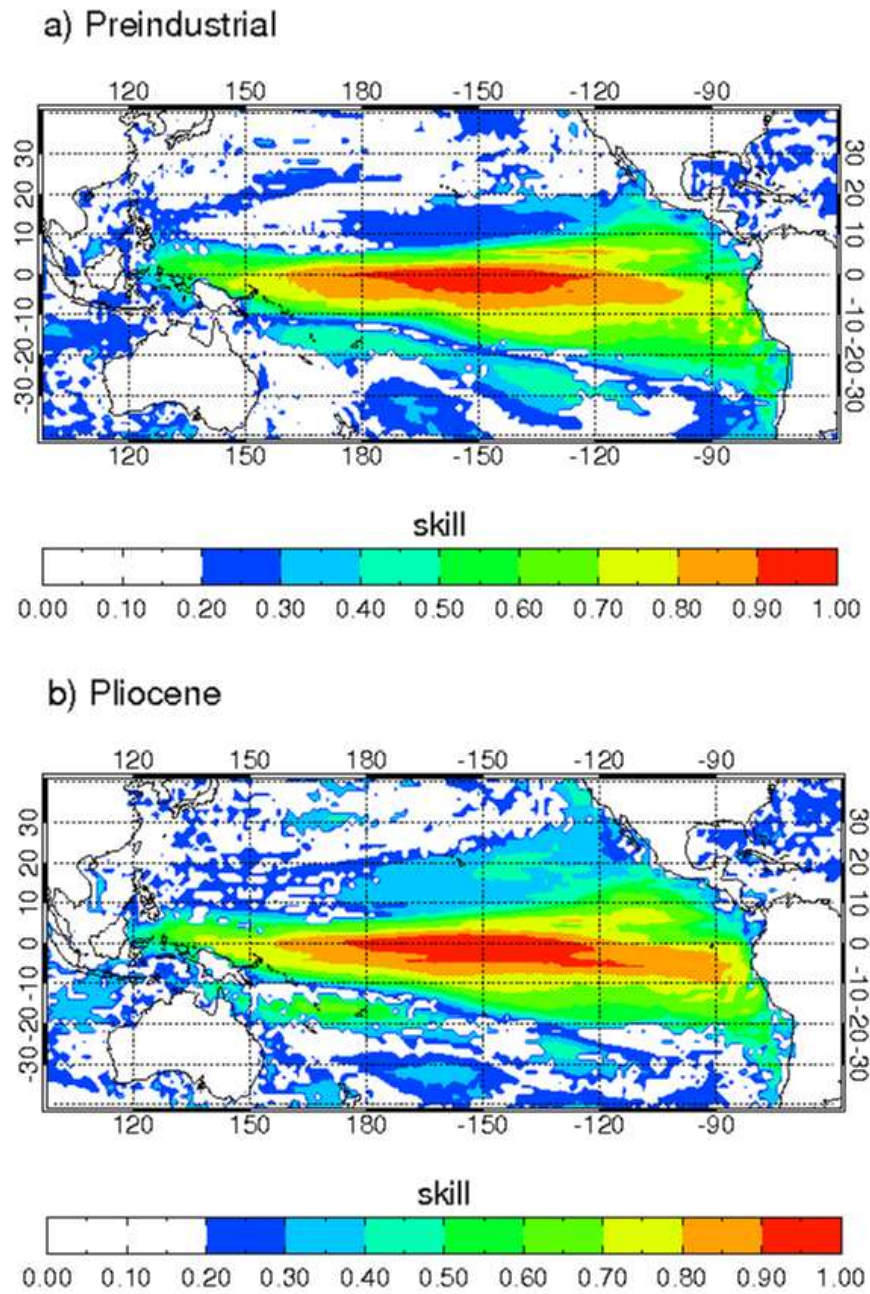


Figure 5. ENSO detection skill for modeled 'pseudocorals' across the Pacific. See section 4.1 for a discussion of how the skill was calculated.

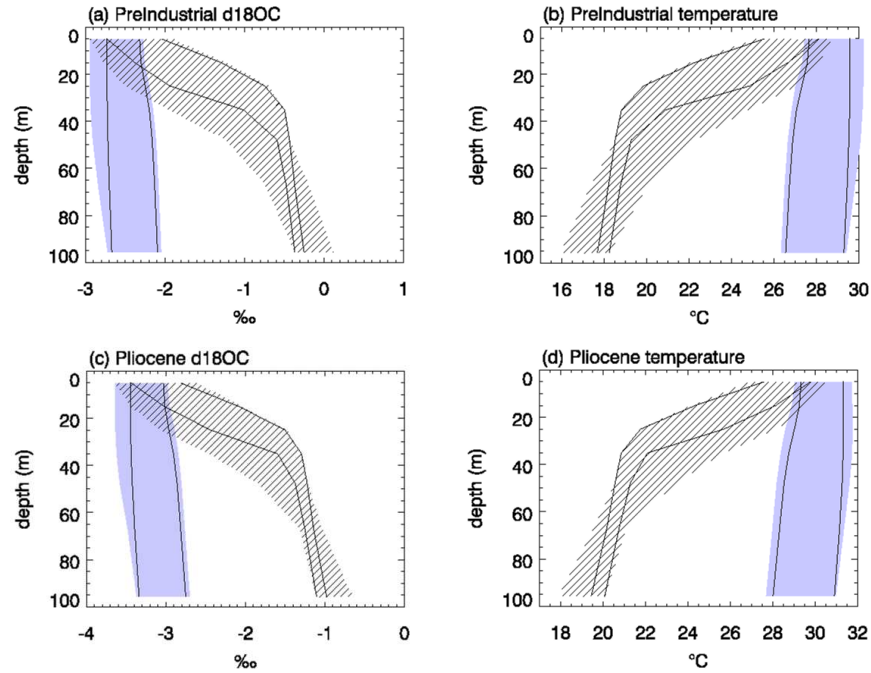


Figure 6. Long term average modeled $\delta^{18}O_F$ and temperature for the preindustrial and mPWP. The blue shaded region shows the range of values within 5.0° of the gridbox containing the western Pacific site (ODP 806) while the hatched region shows the range of values within 5.0° of the gridbox containing the eastern Pacific site (ODP 847). The range of values within 2.5° of each site is shown by the thin black lines.

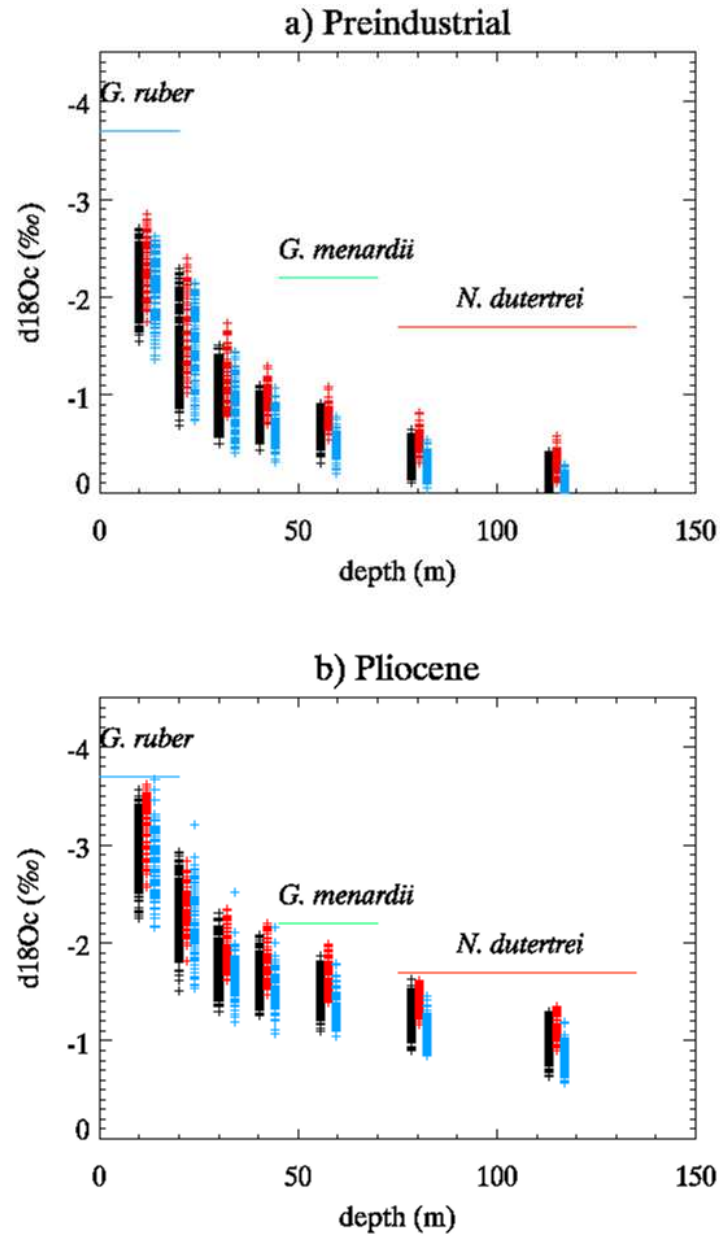


Figure 7. Modeled individual foraminifera (calculated from monthly data) for the last 50 years of the preindustrial (top) and mPWP (bottom) simulations at the gridbox representing ODP846 ($3^{\circ}S$, $90^{\circ}C$). Black crosses represent times when the model was in a neutral state, red crosses represent times when the model was in an El Niño state and blue crosses represent times when the model was in a La Niña state. Different depths are presented to represent results for different foraminifera species.

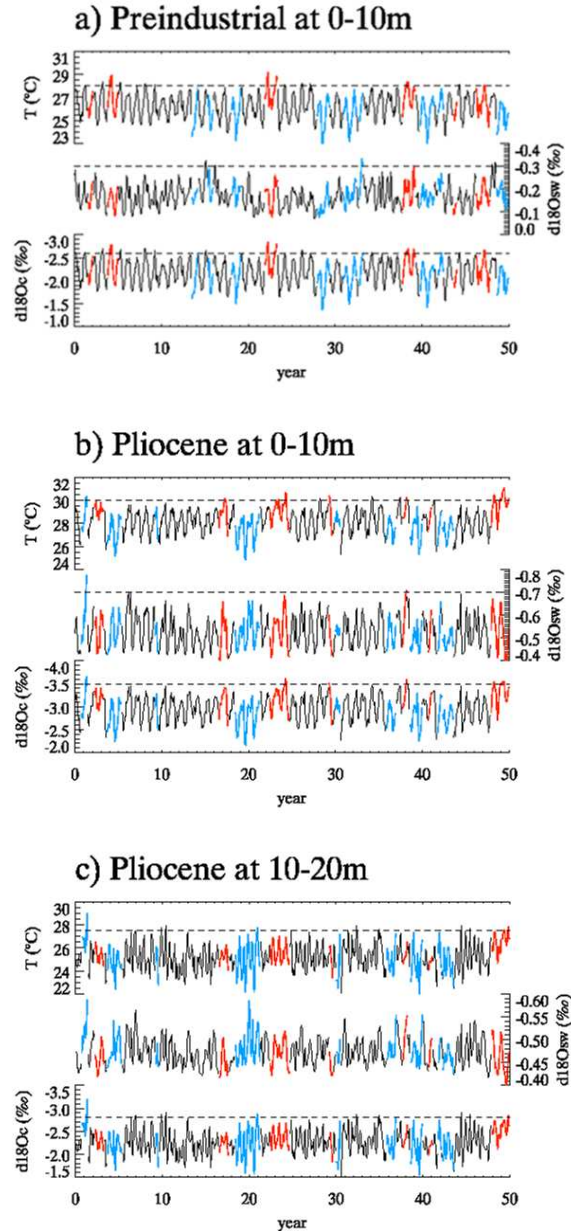


Figure 8. Temperature, $\delta^{18}\text{O}_{sw}$ and $\delta^{18}\text{O}_F$ from the last 50 years of the simulations, for the gridbox containing ODP846 (3°S , 90°W). Red/blue/black shows times when the model is in an El Niño/La Niña/neutral state. Dashed lines are drawn on each figure to highlight ‘extreme’ warm events.

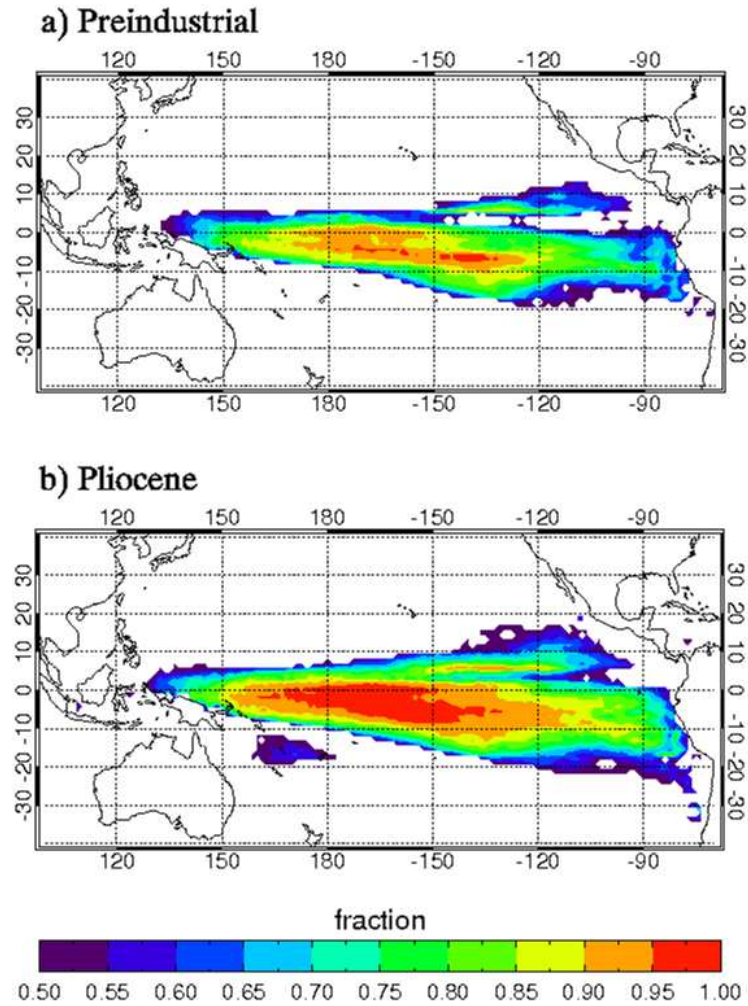


Figure 9. Fraction of the most extreme 2% of pseudo planktonic foraminifera measurements that were correctly attributed to El Niño and La Niña for each location across the Pacific.

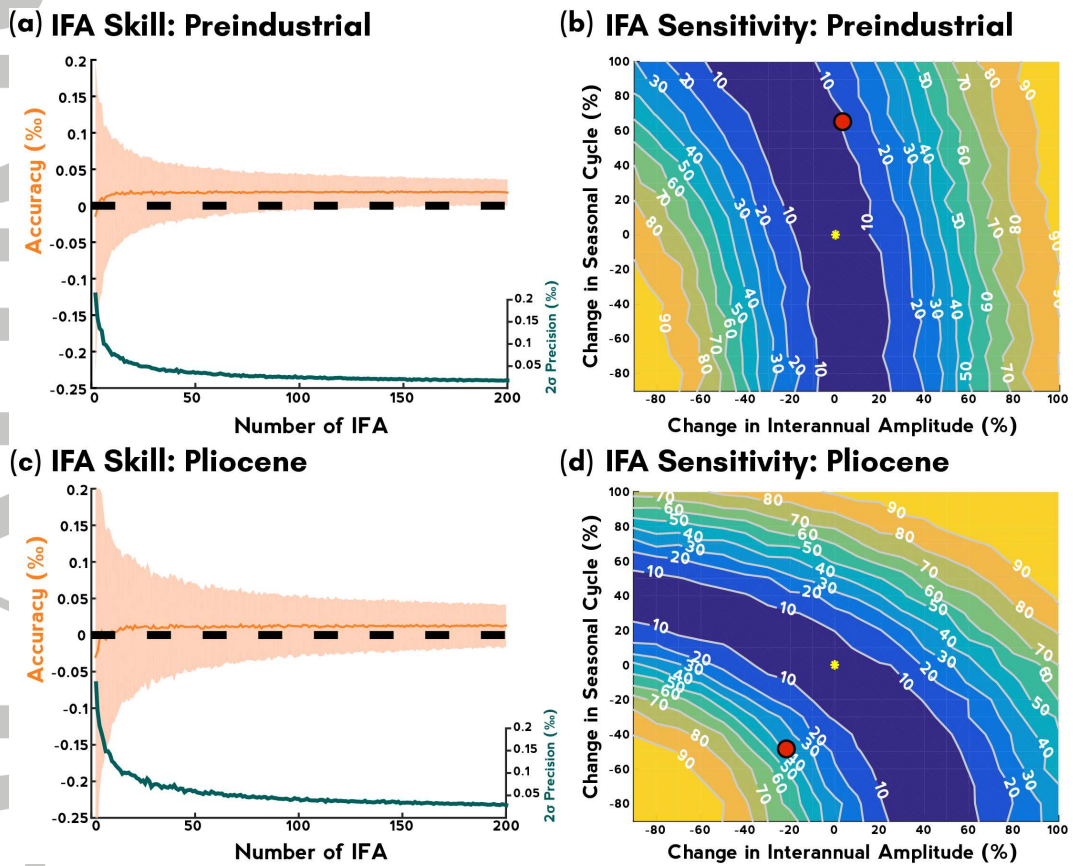


Figure 10. IFA skill and sensitivity for forward modeled *G. ruber* IFA at two sites in the simulated preindustrial (a-b) and mPWP (c-d) oceans using INFAUNAL. (a) Number of individual forams analyzed versus accuracy (orange, %) and precision (green, %) of the standard deviation for 1-200 foraminifera based on preindustrial simulated data at 5,000 Monte Carlo realizations; (b) Probability contour diagram at PreindMax site for 50 foraminifera and a time window of 500 years. (c) and (d) same as in (b) and (c) for the PliMax site. Red circles in (b) and (d) indicate the targets for IFA detection from modeled variability (yellow star).

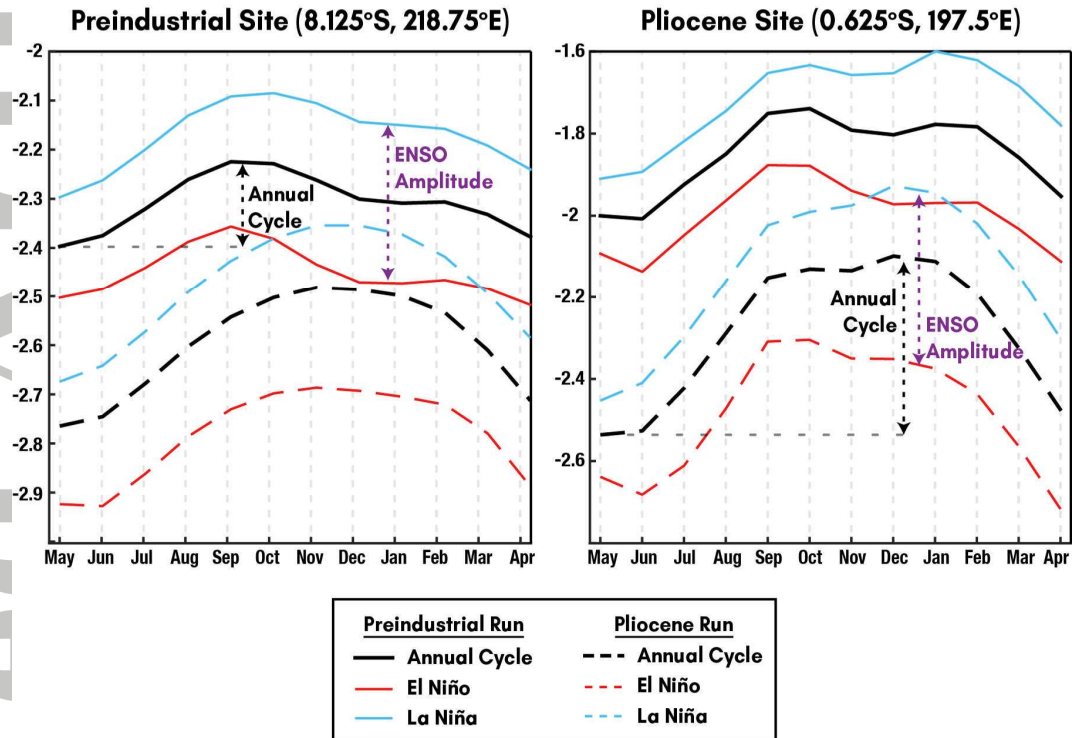


Figure 11. The annual cycle (black), the average El Niño year (red), and the average La Niña year (blue) in the preindustrial simulations (full lines) and mPWP simulations (dashed lines) at the PreindMax site (left) and PlioMax site (right).